Article Title
Railway bridge damage detection using vehicle-based inertial measurements and apparent profile

Authors
Paraic Quirke
Cathal Bowe
Eugene J. OBrien
Daniel Cantero
Pablo Antolin
Jose Maria Goicolea

Manuscript version
Post-print = Final draft post-refereeing, before copy-editing by journal

DOI:
http://dx.doi.org/10.1016/j.engstruct.2017.10.023

Reference:

Quirke, P., Bowe, C., OBrien, E.J., Cantero, D., Antolin, P. Goicolea, J.M. (2017). Railway bridge damage detection using vehicle-based inertial measurements and apparent profile. *Engineering Structures*, 153, pp. 421-442.

Railway bridge damage detection using vehicle-based inertial measurements and apparent profile

Paraic Quirke[1,2], Cathal Bowe[1], Eugene J. OBrien[2], Daniel Cantero[3], Pablo Antolin[4], Jose Maria Goicolea[5]

[1]Iarnród Éireann Irish Rail, Technical Department, Engineering & New Works, Inchicore, Dublin 8, Ireland.
[2]School of Civil Engineering, University College Dublin, Dublin 4, Ireland.
[3]Department of Structural Engineering, Norwegian University of Science & Technology, Trondheim, Norway.
[4]Mathematics Institute of Computational Science and Engineering, École Polytechnique Fédérale de Lausanne, CH-1015 Lausanne, Switzerland.
[5]School of Civil Engineering, Technical University of Madrid, Madrid, Spain.

email: paraic.quirke@irishrail.ie*, cathal.bowe@irishrail.ie, eugene.obrien@ucd.ie, daniel.cantero@ntnu.no, pablo.antolin@epfl.ch, jose.goicolea@upm.es

* corresponding author

ABSTRACT: The presence of damage in a railway bridge alters its stiffness and consequently, its static and dynamic response to loading. The dynamic response of a railway bridge to loading produces a dynamic response in the passing vehicle, potentially enabling detection of the damage through analysis of the vehicle response. A method is proposed in this paper for the detection of bridge damage through comparison of apparent profiles sensed by the passing vehicle. The apparent profile is a virtual longitudinal profile which, when applied to a vehicle, invokes the same measured response to the crossing of a bridge. A change in the deflection of the bridge due to the presence of damage manifests itself as a change in the apparent profile associated with the measured vehicle response.

The Cross Entropy optimisation method is used in this study to determine the apparent profiles that generate a vehicle dynamic response most similar to that of a measured input. 'Measured' bogie vertical acceleration signals are generated using a 3-dimensional train-bridge interaction model implemented in Abaqus and used as input to a 2-dimensional algorithm implemented in Matlab. Damage is introduced to the bridge structure by applying a localised reduction in the width of the bottom flange of a bridge beam, simulating the effect of a sudden impact from a vehicle strike. Apparent profiles for a number of damage scenarios are inferred and compared over time to detect damage. The algorithm is also tested for resilience to sensor noise and effectiveness in the presence of track irregularities.

KEY WORDS: Railway Bridge; Damage; Apparent Profile; Drive by; Vehicle Track Interaction; Cross Entropy, Optimisation.

1.0 INTRODUCTION

The use of vehicle response to determine the condition of railway infrastructure has attracted increased research interest in recent years [1,2]. Sensors attached to in-service trains, coupled with modern communication technologies and data processing techniques have made it possible to provide unattended systems that continuously monitor railway track. However, to the authors' knowledge this is the first time that an unattended drive-by damage detection technique has been proposed for railway bridges.

Railway bridges are critical elements of any railway network. They are expensive to construct and maintain. In the event of serviceability limits being exceeded, or bridge collapse, railway infrastructure owners suffer the cost of both maintenance/replacement and lost revenue during any period of closure. The collapse of the Malahide viaduct in Ireland in 2009, due to undermining of a bridge pier from inter-tidal scouring action, is one such example. The direct cost of replacing the collapsed spans was

approximately € 5m. However the combination of lost revenue and the requirement to provide a replacement bus service cost Irish Rail an additional € 5m [3]. The striking of bridges by large vehicles is considered by Irish Rail to be 'the single most likely cause of a serious rail safety incident on the network' and there were 85 strikes recorded in 2015 alone [4]. In the United Kingdom, Network Rail reported 1,708 bridge strikes to underline bridges in the year ending 31 March 2014 [5]. Structural Health Monitoring (SHM) of railway bridges can help to detect the damage caused by these strikes and aid maintenance planning, thereby helping to prevent bridge collapse, prolong service life and extend the intervals between costly repairs and/or replacements.

Traditionally SHM of railway bridges has been undertaken using periodic visual inspections made by engineers and other technical staff. Owing to the large number of structures present on a typical railway network these methods demand a large number of inspectors resulting in significant cost. This cost is exacerbated by the logistical complications associated with inspections of bridges over water and tall viaducts. It is difficult to achieve consistency in monitoring due to the subjective nature of the inspections. As a result of these and other challenges there has been a shift towards sensor based monitoring with research being conducted into improving sensing technologies and diagnostic techniques [6].

Health monitoring of bridges through analysis of bridge movement measured by sensors can be divided into two types: direct and indirect. Direct monitoring involves attaching sensors directly to the bridge while indirect monitoring involves the placement of sensors on a passing vehicle. A major advantage of indirect monitoring is that an instrumented train can monitor large parts of a network as a by-product of its normal operation. When a vehicle crosses a bridge, the bridge responds with a static deflection coupled with a dynamic oscillation. The presence of damage in the structure causes a change in bridge stiffness which changes the modal properties, influencing both the static and dynamic responses. The response of the bridge is sensed by the passing vehicle which will also behave differently. Consequently, the response of the passing vehicle has the potential to be used to detect damage in the bridge.

Malekjafarian *et al.* [7] present a review of the state-of-the-art for indirect health monitoring of highway bridges. Using vibration-based damage detection methods [8,9], the concept of indirect monitoring of highway bridges was investigated by Yang *et al.* [10,11] and McGetrick [12] and experimentally tested by Lin and Yang [13]. Aside from a paper using wavelet techniques [14] there appears to be little existing literature on indirect damage detection for railway bridges. Track Recording Vehicles are used by railway owners to measure the quality of the track geometry in accordance with European Standards [15]. However, to the authors' knowledge, this information is not currently used to determine the condition of bridge structures supporting the track.

A parametric study conducted by Yang [16] indicates that a large bridge/vehicle acceleration amplitude ratio results in better accuracy in finding bridge frequencies and hence damage. However, to ensure the stability of ballasted track over railway bridges, EN1990 [17] limits the vertical acceleration in the bridge deck to 3.5 m/s^2 (~0.35 g). This low bridge deck vibration limit results in low bridge/vehicle acceleration amplitude ratios meaning that alternatives to frequency based damage detection methods are required to make indirect SHM applications for railway bridges feasible.

Using drive-by techniques to detect changes in bridge natural frequency has other limitations; McGetrick [18] found that low-speeds (less than 5 m/s) are required to enable identification of bridge natural frequencies in the presence of road profile. At higher speeds the influence of the road profile on the bridge excites the vehicle to a greater degree than that of the bridge, making the identification of the bridge natural frequency difficult. The method described in this paper avoids this issue by finding a profile influenced by both the track irregularity and the bridge response.

An additional drawback to frequency domain based techniques is the short duration of the vehicle crossing. The measuring vehicle is not able to record a sufficient number of bridge oscillations during its crossing. The only way to increase the number of bridge oscillations sensed by the passing vehicle, thereby increasing the bridge influence on the vehicle response, is to reduce the vehicle speed.

Frequency identification based methods such as Fourier transforms require long signals to accurately extract bridge frequencies. It is not reasonable to expect in-service trains to travel at low speeds across bridges for the purposes of SHM. Therefore these frequency based methods may not be suitable for railway applications.

Some researchers have combined optimisation techniques with direct measurement of railway bridges to detect damage. He *et al.* [19] use a genetic algorithm optimisation technique to identify the location and magnitude of railway bridge damage using an inverse analysis of the vehicle-bridge interaction. A range of bridge damage scenarios are optimised to find the scenario that produces a vehicle response most similar to a measured response. Shu *et al.* [20] propose a bridge damage detection methodology using bridge displacement and acceleration as input to a trained back-propagation artificial neural network. OBrien and Keenahan [21] use pavement deflection readings taken by a passing vehicle to determine apparent profile through cross-entropy optimisation for damage detection in highway bridges. Elhattab *et al.* [22] use a similar method to show that the bridge displacement profile, calculated through comparison of apparent profiles to a baseline profile, is sensitive to varying levels of bridge damage. However it is found that the bridge displacement profile difference is contaminated by the effect of the road profile when variation in the transverse position of the wheel path across the bridge is taken into account. In adapting the apparent profile method for detection of damage in railway bridges one can make use of the fact that lateral positioning of the vehicle on the bridge changes by a negligible amount (only by the hunting motion due to conicity of the wheelsets) as it is guided across the bridge along the rails.

In this paper the methodology described in OBrien *et al.* [23] is used to infer apparent profiles from vehicle inertial response to crossing a railway bridge. Damage is applied and the resulting apparent profiles are compared to determine if they are damage-sensitive. The area computed between a zero elevation and the apparent profile across the bridge is used as the damage indicator.

2.0 MODEL DESCRIPTION

It is not feasible to implement an experimental testing programme in which a bridge is damaged. 'Measurements' of vehicle response to crossing of the healthy and damaged bridge are therefore generated here by simulation. On the other hand, using the same model to generate 'measurements' and at the same time to detect damage using these 'measurements' would neglect the influence of model uncertainty. To address this issue, two models are used in this study. Vehicle response is generated using a 3-dimensional train-bridge interaction model implemented in the Abaqus finite element software package [24]. The outputs of this model are used as input into a 2-dimensional Matlab model to determine whether the apparent profiles are damage-sensitive.

2.1 3D Bridge Model

A 3-dimensional non-linear coupled train-bridge dynamic interaction model is used to numerically generate vehicle response to a bridge crossing event. The vehicle is a multi-body system with parameters based on the Siemens AVE S-103 (ICE3 Velaro E) high speed train as described by Nguyen *et al.* [25] with some minor amendments to vehicle properties according to Goicolea [26]. The interaction between the vehicle and the structure is described in Section 2.2.

The bridge model used in the interaction is a finite element model, based on a reinforced concrete beam and slab bridge situated on the Madrid-Barcelona high-speed railway line as described by Martínez-Corcoba [28] (1). The double-tracked (standard 1435 mm gauge) bridge crosses the Rio Torote approximately 25 km east of Madrid. The 72.8 m long bridge consists of four spans: two 20 m central spans and two 16 m side spans next to the abutments. All spans are simply supported, resting on neoprene pads fixed to the top of reinforced concrete piers. The 0.25 m thick reinforced concrete deck is connected to four pre-tensioned reinforced concrete I-beams using shear bolts to create a composite structure.

Figure 1. Rio Torote railway bridge (from Martínez-Corcoba [28]**)**

Martínez-Corcoba [28] develops a simplified 3 dimensional finite element model of the bridge side-span for the study of dynamic effects during the passage of trains. This model is used here despite the fact that the behaviour of a single span will not be an accurate match of one span of the actual bridge. It is used here to determine the sensitivity of the method to damage and is assumed that similar levels of sensitivity can be found in an actual bridge. The bridge deck is modelled using a mesh of S4R5 shell elements, 1.34 m square and 0.25 m thick. Abaqus S4R5 elements are Kirchhoff-Love stress/displacement shell elements consisting of 4 nodes with 5 DOF per node and reduced integration. The bridge deck mesh is 8 elements wide and 12 elements in length, representing a bridge 10.72 m wide and 16.08 m in length. The beams are linked with the appropriate offset to the bottom surface of the deck, modelled using Abaqus B31 type beam elements (3 dimensional, shear flexible, using first-order interpolation functions) with an I-section. Other bridge properties are listed in **Error! Reference source not found.**.

Table 1. Properties of 3D bridge model

Property	Unit	Symbol	Value
Deck – Density of reinforced concrete*	kg/m^3	ρ_d	6 594
Deck – Poisson ratio	-	ν_d	0.25
Deck – Modulus of elasticity	GPa	E_d	33
Beam – Density of reinforced concrete	kg/m^3	ρ_b	2 500
Beam – Poisson ratio	-	ν_b	0.25
Beam – Modulus of elasticity	GPa	E_b	37
Beam – Full depth	m	h	1.36
Beam – Width of bottom flange	m	b_1	1.2
Beam – Width of top flange	m	b_2	0.6
Beam – Thickness of bottom flange	m	t_1	0.2
Beam – Thickness of top flange	m	t_2	0.2
Beam – Thickness of web	m	t_3	0.15
Bridge section – 2nd moment of area	m^4	I_{yy}^t	1.48

* Includes allowance for ballast and track elements contributing to deck self-weight.

Damage is modelled as a symmetrical reduction in the width of the bottom flange of a beam element to simulate the effect of a vehicle striking the bridge while passing underneath. **Error! Reference source not found.** details the effect of the reduction on the 2nd moment of area for the individual beam element, the composite beam-slab section (consisting of the beam element and two deck shell elements) and the overall bridge cross-section (four beam elements and 8 deck shell elements).

Table 2. Damage levels

Damage Level	b_1 (m)	I_{yy}^b (Beam) (m^4)	% Reduction	I_{yy}^c (Composite) (m^4)	% Reduction	I_{yy}^t (Total) (m^4)	% Reduction
Healthy	1.2	0.12	-	0.37	-	1.48	-
Damage I	0.65	0.10	22.5 %	0.26	30 %	1.37	7.5 %
Damage II	0.2	0.06	53 %	0.15	60 %	1.26	15 %

2.2 3D train-bridge interaction model

The dynamic interaction between the bridge model (described in Section 2.1), and the vehicle, modelled as a multi-bodied system, is based on a simplification of the interaction described in Antolin *et al.* [27]. Since the measurement of the response of the bogie frame is of interest in this study, elements of the model remote from that location can be treated in a simpler way. Therefore, the Hertzian wheel-rail contact algorithm used in the interaction model described by Antolin *et al.* [27] is replaced by a simplified rigid connection thereby reducing the computational effort required.

To establish the interaction between the vehicle and the structure, every axle of the train is kinematically coupled to the bridge deck. The enforcement of these kinematic relationships establishes the dynamic interaction between the two subsystems: the structure reaction forces are transmitted to the axles of the vehicle and vice versa.

The key components for establishing the kinematic relationships are illustrated in Figure 2 and Figure 3. The kinematics of every vehicle wheelset is described by the node W, the centre of mass of the rigid body modelling the wheelset. The nodes W are constrained to follow the trajectory defined by the bridge deck deformation. Thus, in order to describe this path, a point D and a node T are introduced for each vehicle wheelset (for kinematic purposes only, see Figure 3).

The point D associated to each wheelset follows the trajectory defined by the line of nodes in the bridge finite element model corresponding to the track centre-line, as shown in Figure 2 and Figure 3. This trajectory is not fixed, but moves according to the bridge deck deformation. Thus, at each longitudinal co-ordinate, s, the point D is situated on the edge shared by the two shell elements of the deformable concrete slab. If N_1 and N_2 are the two nodes of that edge for a certain section, s, the position and rotation of point D is computed by interpolating linearly the positions and rotations of the nodes as:

$$r_D = \xi r_{N_1} + (1-\xi) r_{N_2} \tag{1a}$$

$$\theta_D = \xi \theta_{N_1} + (1-\xi) \theta_{N_2} \tag{1b}$$

where r and θ are the position and rotation vectors corresponding to the point D and the nodes N_1 and N_2; while ξ is the relative longitudinal coordinate with respect to N_1, i.e. $\xi(s) = (s - s_1)/(s_2 - s_1)$, where s_1 and s_2 are the longitudinal positions of the shell nodes. It is important to note that, in principle, to interpolate rotations linearly as it is done in Equation (1b) is incorrect. However, due to the fact that the bridge rotations are expected to be small, the error made in the interpolation will also be small.

The nodes Tdescribe the kinematics of the central point of the track as the bridge deforms. Their positions and rotations are computed as an offset with respect to the points D:

$$r_T(s) = r_D(s) + \rho_{DT}(s) + \theta_D(s) \times \rho_{DT}(s) \tag{2a}$$

$$\theta_T(s) = \theta_D(s) \tag{2b}$$

where $\rho_{DT}(s)$ is the offset vector between points D and T given by:

$$\rho_{DT}(s) = \rho_{DT}^0 + \Gamma(s) \tag{3}$$

where Γ is a vector describing the track irregularity at track longitudinal coordinate s, and ρ_{DT}^0 is the offset vector between points D and T when a perfect track with no irregularities is considered. As detailed in Section 2.3, only vertical track irregularities are considered in this work.

Since no there is no wheel-rail interaction in the model, nodes W are assumed to be rigidly connected to the track at every position, i.e. to the nodes T. Thus, the position and rotation of W is computed as an offset with respect to node T:

$$r_W(s) = r_T(s) + +\theta_T(s) \times \rho_{TW}^0(s) \tag{4a}$$

$$\theta_W(s) = \theta_T(s) = \theta_D(s) \tag{4b}$$

where ρ_{TW}^0 is the offset vector between the nodes T and W which is considered to be constant. It is seen in the equation above that it is assumed that the rotation of the vehicle wheelset at a section s is defined by the rotation of T, and therefore is equal to the rotation of the bridge slab at that longitudinal position.In order to impose the kinematic relationships described by Equations (2) and (4), user defined multi-point constraints are implemented in the Abaqus model.

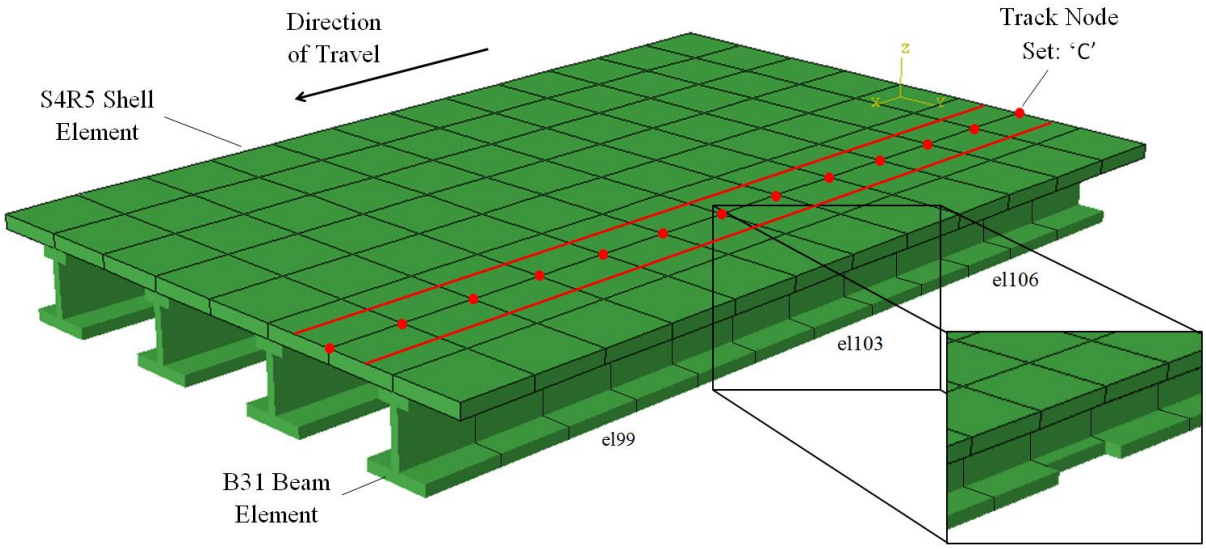

Figure 2. Abaqus bridge model in healthy condition; application of damage (reduction in width of bottom flange) in beam element 103 shown in inset

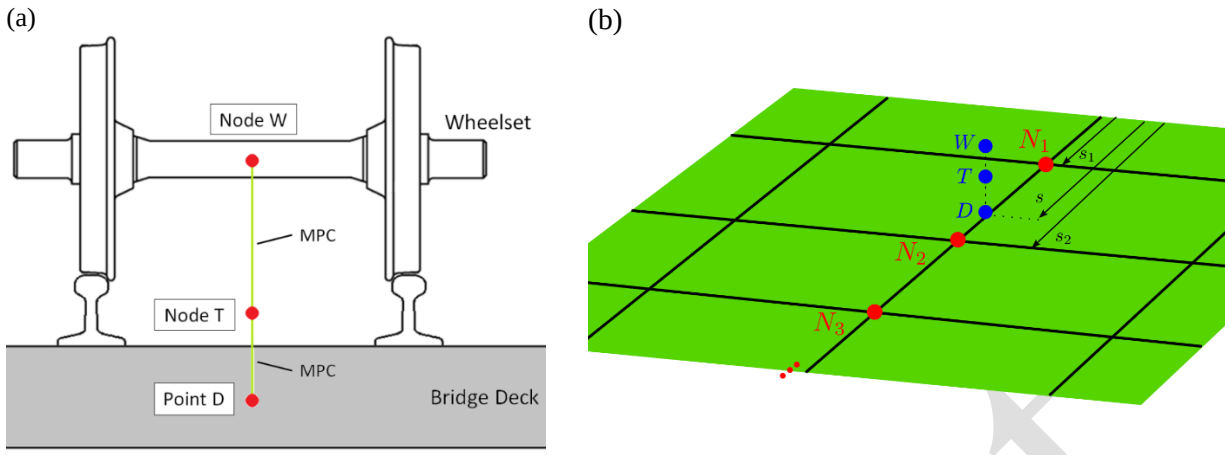

Figure 3. Vehicle-bridge kinematic interaction. a) Enforcement of kinematic constraints between vehicle and structure by means of multi-point constraints (MPC). b) Description of the position of the track and vehicle wheelsets relative to the bridge shell elements.

The interaction simulation is divided into three main steps. Initially, the vehicle is placed on a rigid platform and allowed to attain dynamic equilibrium under its self-weight for a simulated period of 10 s. Secondly, the vehicle is uniformly accelerated to the final stationary velocity. While maintaining dynamic equilibrium, the vehicle approaches the bridge along the rigid platform for a simulated period of 20 s. Following this, the leading axle of the train enters the bridge. The interaction is terminated once the trailing axle of the train has left the bridge.

If track irregularities are being considered in the interaction, they are randomly generated for the track section between a point 5 m before the bridge and a point 5 m beyond the bridge. In addition, two transition sections, each 5 m in length, are provided to ensure a smooth transition from zero elevation to and from the track irregularities.

2.3 Track Irregularity Profile

As stated in model description, a track irregularity is considered at node T in the interaction between the vehicle and the bridge. This vertical track irregularity is interpolated from a longitudinal track profile, randomly generated using a Power Spectral Density (PSD) function [29]:

$$S(\Omega) = \frac{A_v \Omega_c^2}{(\Omega^2 + \Omega_r^2)(\Omega^2 + \Omega_c^2)} \tag{3}$$

where Ω is the spatial frequency, and coefficients A_v, Ω_r and Ω_c, relate to the grade of track. In this paper, irregularities are generated within a wavelength range D1, as defined in EN13848 [15], requiring a minimum wavelength of 3 m and a maximum wavelength of 25 m. A 'Class 6' profile is used in the simulations which represents a track of 'Moderate' quality giving $A_v = 1.5 \times 10^{-6}$, $\Omega_r = 0.0206$ rad/s and $\Omega_c = 0.825$ rad/s. The irregularity profile used in this paper is presented in tabular form in Appendix A.

2.4 2D Interaction Model

This section describes the 2-dimensional vehicle-track interaction model used to infer apparent profiles for the purposes of damage detection in bridges. As the interaction model is employed in an optimisation technique, a simplified 2D model is required to maximise the efficiency of the optimisation. The car vehicle model presented in this section is used widely in the literature [30–32]. Nguyen found that 2D models can sufficiently predict vertical dynamic response [25]. Using a 2D vehicle model to fully represent a 3D system means that only a single track profile can be inferred. This

extracted profile corresponds to an average of the two rail profiles. The track itself is considered to be infinitely stiff, i.e. no deformation is permitted.

The 2D car vehicle model is shown in Figure 3. The development of this vehicle model is detailed in Cantero *et al.* [33] who provide some commentary on vehicle properties. A brief description of the model is provided here. The multi-body model consists of a main body and two bogies represented by rigid bars. The bogies are each connected to the main body by a spring and damper representing the secondary suspension system. The wheelsets are represented as lumped masses and are connected to the bogies by means of a spring damper system representing the primary suspension. Considering vertical translation and rotation about the centre of gravity for the car body and bogies, and vertical translation for each wheelset, the model contains 10 degrees of freedom (DOF). The wheels are fixed to the track with no separation being permitted. This reduces the system to 6 DOF. Vehicle properties are for the Siemens ICE3 Velaro high-speed train [26] and are listed in Table 3.

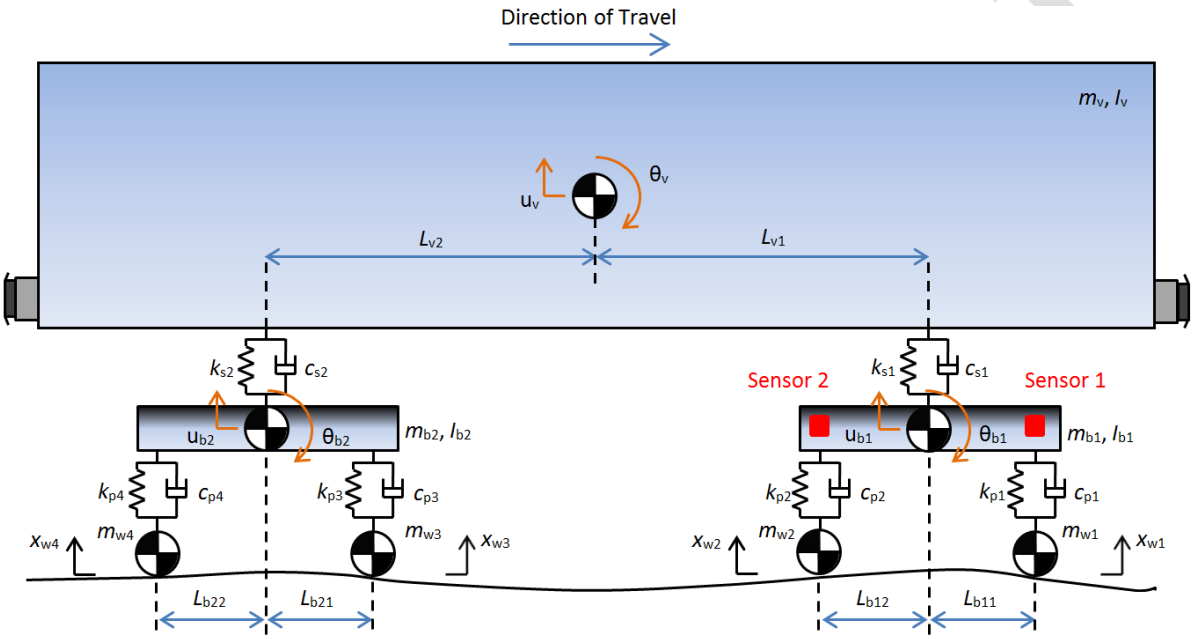

Figure 3. Model B: 2D car vehicle and sensor locations (see Table 3 for description of symbols)

Table 3. Mechanical properties of the 2D car vehicle (ICE3 Velaro)[26]

Property	Unit	Symbol	Value
Mass of wheelset	kg	$m_{w1}, m_{w2}, m_{w3}, m_{w4}$	1 800
Mass of bogie	kg	m_{b1}, m_{b2}	3 500
Mass of main body	kg	m_v	47 800
Moment of inertia of bogie	kg.m^2	J_{b1}, J_{b2}	1 715
Moment of inertia of main body	kg.m^2	J_v	1.96×10^6
Stiffness of primary suspension	N/m	$k_{p1}, k_{p2}, k_{p3}, k_{p4}$	2.4×10^6
Stiffness of secondary suspension	N/m	k_{s1}, k_{s2}	0.7×10^6
Damping of primary suspension	Ns/m	$c_{p1}, c_{p2}, c_{p3}, c_{p4}$	20×10^3
Damping of secondary suspension	Ns/m	c_{s1}, c_{s2}	40×10^3
Distance between main body centre of gravity and bogies	m	L_{v1}, L_{v2}	8.6875
Distance between bogie centre of gravity and wheelsets	m	$L_{b11}, L_{b12}, L_{b21}, L_{b22}$	1.25

Assuming small rotations, a linearised system of equations of motion is adopted, which is, in matrix form:

$$\mathbf{M_v}\ddot{u} + \mathbf{C_v}\dot{u} + \mathbf{K_v}u = F \tag{4}$$

where M_v, C_v and K_v are the mass, damping and stiffness matrices of the vehicle respectively. The vectors $\ddot{u}$, $\dot{u}$, u and F contain the vehicle accelerations, velocities, displacements and external forces respectively. All matrices and vectors are defined in the following equations:

$$\mathbf{M_v} = diag[m_v \quad m_{b1} \quad m_{b2} \quad I_v \quad I_{b1} \quad I_{b2}] \tag{5}$$

$$\mathbf{K_v} = \begin{bmatrix} k_{s1}+k_{s2} & -k_{s1} & -k_{s2} & L_{v1}k_{s1}-L_{v2}k_{s2} & 0 & 0 \\ -k_{s1} & k_{p1}+k_{p2}+k_{s1} & 0 & -L_{v1}k_{s1} & L_{b11}k_{p1}-L_{b12}k_{p2} & 0 \\ -k_{s2} & 0 & k_{p3}+k_{p4}+k_{s2} & L_{v2}k_{s2} & 0 & L_{b21}k_{p3}-L_{b22}k_{p4} \\ L_{v1}k_{s1}-L_{v2}k_{s2} & -L_{v1}k_{s1} & L_{v2}k_{s2} & {L_{v1}}^2k_{s1}+{L_{v2}}^2k_{s2} & 0 & 0 \\ 0 & L_{b11}k_{p1}-L_{b12}k_{p2} & 0 & 0 & {L_{b11}}^2k_{p1}+{L_{b12}}^2k_{p2} & 0 \\ 0 & 0 & L_{b21}k_{p3}-L_{b22}k_{p4} & 0 & 0 & {L_{b21}}^2k_{p3}+{L_{b22}}^2k_{p4} \end{bmatrix} \tag{6}$$

$$\mathbf{C_v} = \begin{bmatrix} c_{s1}+c_{s2} & -c_{s1} & -c_{s2} & L_{v1}c_{s1}-L_{v2}c_{s2} & 0 & 0 \\ -c_{s1} & c_{p1}+c_{p2}+c_{s1} & 0 & -L_{v1}c_{s1} & L_{b11}c_{p1}-L_{b12}c_{p2} & 0 \\ -c_{s2} & 0 & c_{p3}+c_{p4}+c_{s2} & L_{v2}c_{s2} & 0 & L_{b21}c_{p3}-L_{b22}c_{p4} \\ L_{v1}c_{s1}-L_{v2}c_{s2} & -L_{v1}c_{s1} & L_{v2}c_{s2} & {L_{v1}}^2c_{s1}+{L_{v2}}^2c_{s2} & 0 & 0 \\ 0 & L_{b11}c_{p1}-L_{b12}c_{p2} & 0 & 0 & {L_{b11}}^2c_{p1}+{L_{b12}}^2c_{p2} & 0 \\ 0 & 0 & L_{b21}c_{p3}-L_{b22}c_{p4} & 0 & 0 & {L_{b21}}^2c_{p3}+{L_{b22}}^2c_{p4} \end{bmatrix} \tag{7}$$

$$\ddot{u} = \begin{Bmatrix} \ddot{u}_v \\ \ddot{u}_{b1} \\ \ddot{u}_{b2} \\ \ddot{\theta}_v \\ \ddot{\theta}_{b1} \\ \ddot{\theta}_{b2} \end{Bmatrix} \tag{8}$$

$$\dot{u} = \begin{Bmatrix} \dot{u}_v \\ \dot{u}_{b1} \\ \dot{u}_{b2} \\ \dot{\theta}_v \\ \dot{\theta}_{b1} \\ \dot{\theta}_{b2} \end{Bmatrix} \tag{9}$$

$$u = \begin{Bmatrix} u_v \\ u_{b1} \\ u_{b2} \\ \theta_v \\ \theta_{b1} \\ \theta_{b2} \end{Bmatrix} \tag{10}$$

$$F = \begin{Bmatrix} m_v g \\ m_{b1}g + k_{p1}r_{w1} + c_{p1}r'_{w1} + k_{p2}r_{w2} + c_{p2}r'_{w2} \\ m_{b2}g + k_{p3}r_{w3} + c_{p3}r'_{w3} + k_{p4}r_{w4} + c_{p4}r'_{w4} \\ 0 \\ L_{b11}(k_{p1}r_{w1} + c_{p1}r'_{w1}) - L_{b12}(k_{p2}r_{w2} + c_{p2}r'_{w2}) \\ L_{b21}(k_{p3}r_{w3} + c_{p3}r'_{w3}) - L_{b22}(k_{p4}r_{w4} + c_{p4}r'_{w4}) \end{Bmatrix} \tag{11}$$

where g is acceleration due to gravity (9.81 m/s^2) while r_{w1}, r_{w2}, r_{w3} and r_{w4} are the track profile elevations under each axle. The dynamic equations of motion of the system are solved using the Wilson-

θ integration method [34,35] and implemented in Matlab [36]. The value of the parameter, $\theta = 1.420815$ is used for unconditional stability in the integration scheme [37].

3.0 METHODOLOGY

Any method for finding bridge damage requires the identification of an indicator that is damage sensitive (e.g. bridge frequency, damping, mode shapes, curvature). In this paper the apparent profile is tested as a damage indicator. An apparent profile is a virtual longitudinal profile which generates a vehicle response matching the measured response of the vehicle. The computation of apparent profile is an inverse problem where a measured output (e.g. acceleration) is used as input to an optimisation algorithm.

OBrien *et al.* [23] developed a method employing cross-entropy combinatorial optimisation to infer track longitudinal profiles. A similar methodology is used in this work however the track model is not allowed to deflect; i.e. the track is infinitely stiff.. A 3D vehicle track interaction (VTI) is used to generate a measured reference signal prior to initiating an optimisation algorithm to find the track profile. The method to find the apparent profile from the measured reference signal initially requires the generation of a population of trial track profiles which are randomly generated using an initial mean and standard deviation for a number of elevations. VTIs are carried out for each. The resulting bogie vertical acceleration signals for each trial profile are compared to the measured reference signal using an optimisation function and ranked. The trial profiles resulting in the best objective function values are used to generate the next, improved population of trial profiles. The method iterates until convergence to a track profile which generates a vehicle response most similar to the measured reference signal.

The objective function used in the optimisation is different to that used in OBrien *et al.* [23]. It is found that during bridge crossing events the deflection of the bridge at a point is different when following axles cross that same point in space. Therefore it is required to find two apparent profiles, one for each axle on the instrumented bogie. The effect of the axles on the second bogie crossing is damped out by 3 levels of suspension and it therefore has a negligible contribution to the vibration of the first (instrumented) bogie. The sensor positions are on the bogie frame in line with the axle axis as shown in Figure 3.

Similar to OBrien *et al.* [23] an objective sub-function is used due to the time-space discretisation resulting in a set of state vectors for each elevation in the rail profile. In this method the i^{th} objective sub-function O_i, is calculated for each value i of bogie vertical acceleration at Sensor 1, $\ddot{u}_1$, and Sensor 2, $\ddot{u}_2$:

$$O_i = \left(\ddot{u}_{1,i} - \ddot{u}^{\circ}_{1,i}\right)^2 + \left(\ddot{u}_{2,i} - \ddot{u}^{\circ}_{2,i}\right)^2 \tag{12}$$

where the reference signal is denoted by the superscript '°'. The number of unknowns (elevations) in a profile on a bridge is a function of the bridge span, the speed of the vehicle and the sensor scan rate. To reduce the dimensionality of the optimisation problem, and increase the likelihood of convergence, it is required to limit the number of unknowns. This is achieved by splitting the profile into a number of phases each containing a lesser number of unknowns. The optimisation problem is solved within the phase before stepping on to the next phase. The inferred profile found in the previous phase is used to generate the estimates for the next phase with a 50% overlap between the phases. The flowchart in Figure 4 summarises the overall process of finding the apparent profile using vertical acceleration as input while Figure 5 describes the method of finding a section of the apparent profile within a phase. Table 4 lists the parameters used in the Cross Entropy optimisation method.

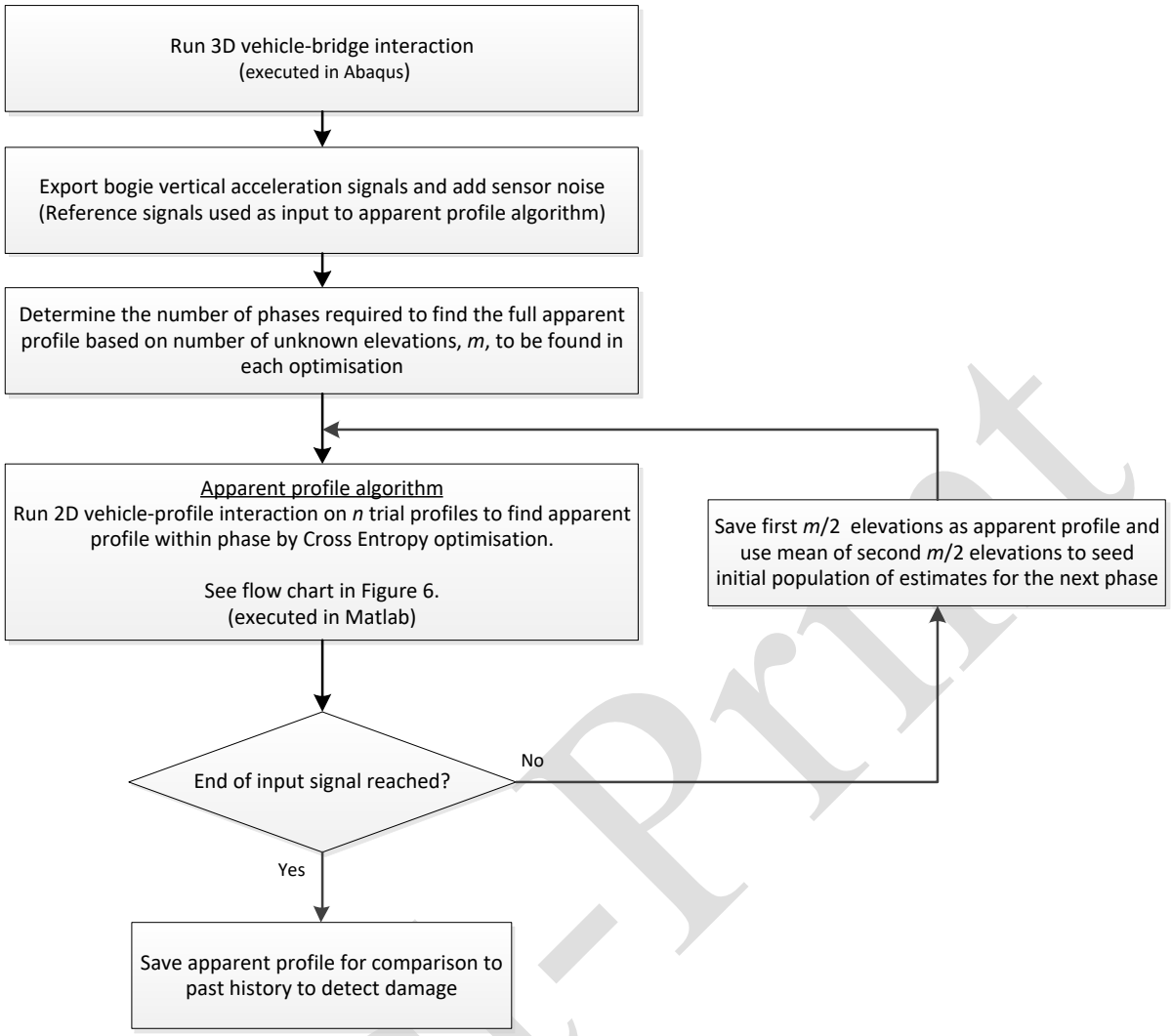

Figure 4. Flowchart describing methodology for finding apparent profile

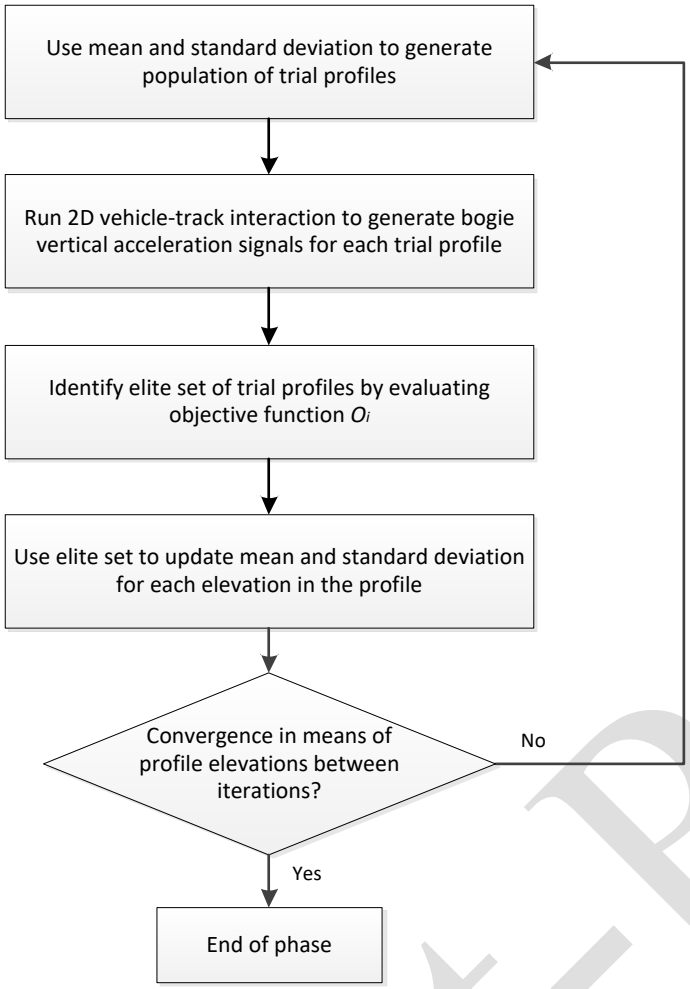

Figure 5. Flowchart describing apparent profile algorithm

Table 4. Cross Entropy optimisation parameters

Property	Value
Length of profile inferred per phase	1.67 m
Number of unknown elevations in each phase (m)	16
Initial mean (μ)	0
Initial standard deviation (σ)	1 mm
Size of each population of estimates (n)	100
Size of elite set (percentage of population of estimates)	10 %
Convergence threshold (within phase)	5×10^{-11}

3.1 Damage Indicator

In this study the presence of damage in a bridge is detected by finding changes in the apparent profile. It is found that using a comparison between profile elevations at one point in particular (e.g. at mid-span) is an unreliable indicator as it is only one point and the differences between profiles may be greater at other locations on the bridge. To account for differences between apparent profiles over the entire bridge span, an area between zero elevation and the apparent profile is computed and used as the damage indicator. A change in the value of this area will indicate that a change has occurred somewhere along the apparent profile. The highlighted region in Figure 6 shows the area used as the damage indicator.

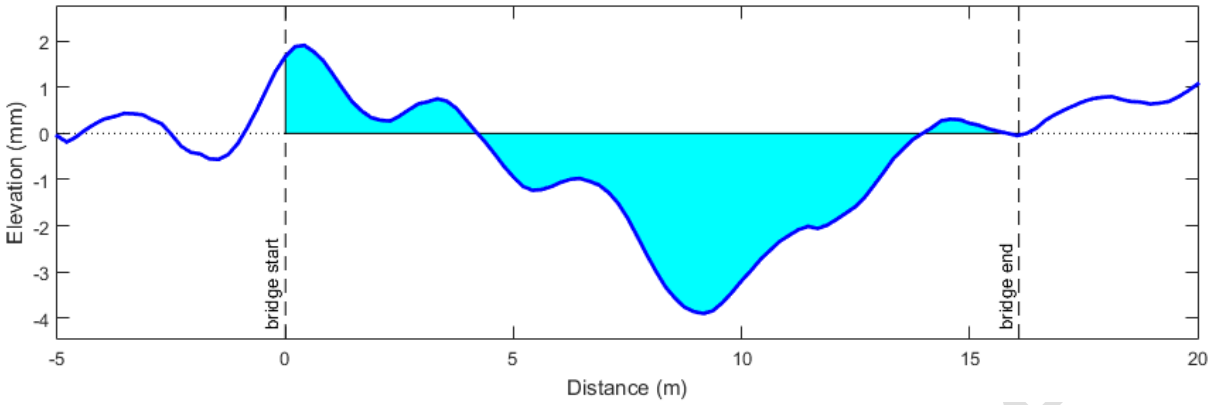

Figure 6. Area between zero elevation and apparent profile on bridge

4.0 RESULTS AND DISCUSSION

The results of a number of numerical tests for the detection of bridge damage using the apparent profile method are presented in this section. The capability of the method is tested for various combinations of damage scenarios (varying damage location and magnitude), effectiveness in the presence of track irregularities and two levels of added sensor noise. The damage scenarios considered are listed in Table 5. Vehicle-bridge interaction modelling these scenarios is executed in Abaqus in order to generate the reference acceleration signals used as input into the apparent profile algorithm. The vehicle is modelled travelling at a constant speed of 150 km/h (41.6 m/s) in all scenarios. A sensor scan rate of 200 Hz is used. Reference acceleration signals generated for each scenario are tabulated in Appendix B.

Table 5. Damage Scenarios (Refer to Figure 2 for element numbers)

Scenario	Damage location	Damage magnitude (I_{yy}^{t})	Irregularities
A	el103 (mid-span)	I (7.5 %)	No
B	el103 (mid-span)	II (15 %)	Yes
C	el106 (1/4-span)	II (15 %)	Yes
D	el 99 (3/4-span)	II (15 %)	Yes

4.1 Scenario A

In order to demonstrate the capability of the apparent profile to detect the deflection of a bridge, a simplified scenario is modelled. The vehicle bridge interaction is carried out on a perfectly level track (i.e. no vertical track irregularities are considered). Therefore the excitation and hence elevation of the apparent profile is due to the total deflection (static and dynamic) of the bridge only. Figure 7 shows the deflection of the bridge model at mid-span of the 'C' node set (see **Error! Reference source not found.**). The bridge deflects by 1.23 mm under the load of the leading bogie of the first coach in the train.

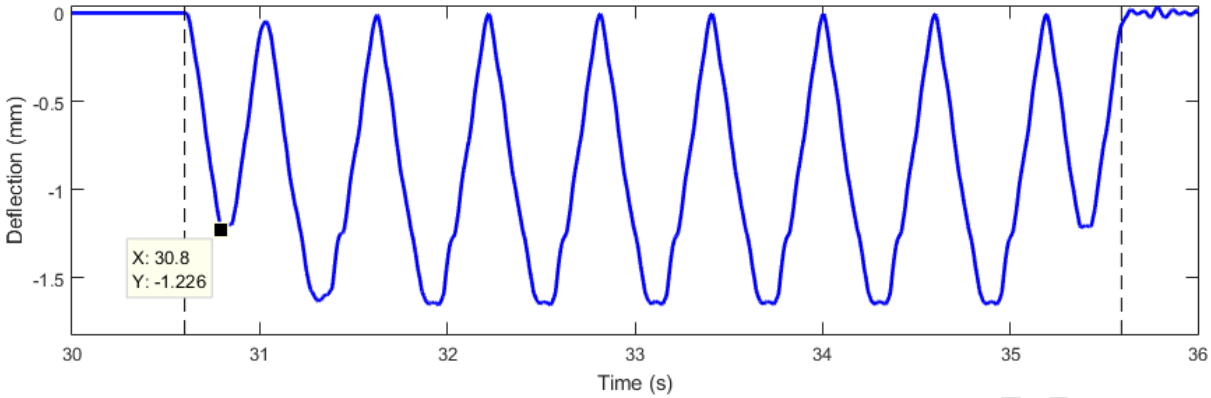

Figure 7. Scenario A: Deflection of track centreline node C at mid-span on healthy bridge due to 8 carriage train. Vertical dashed lines represent the entry and exit of the train

Figure 8 shows the reference signals generated by the 3D interaction model for Sensors 1 and 2. The differences between the signals for the healthy bridge and damaged bridges are quite small (maximum difference 0.06 m/s^2 or 0.006 g). The magnitude of the differences suggests that highly sensitive accelerometers with low levels of noise are required to enable detection of the level of bridge damage considered in this scenario.

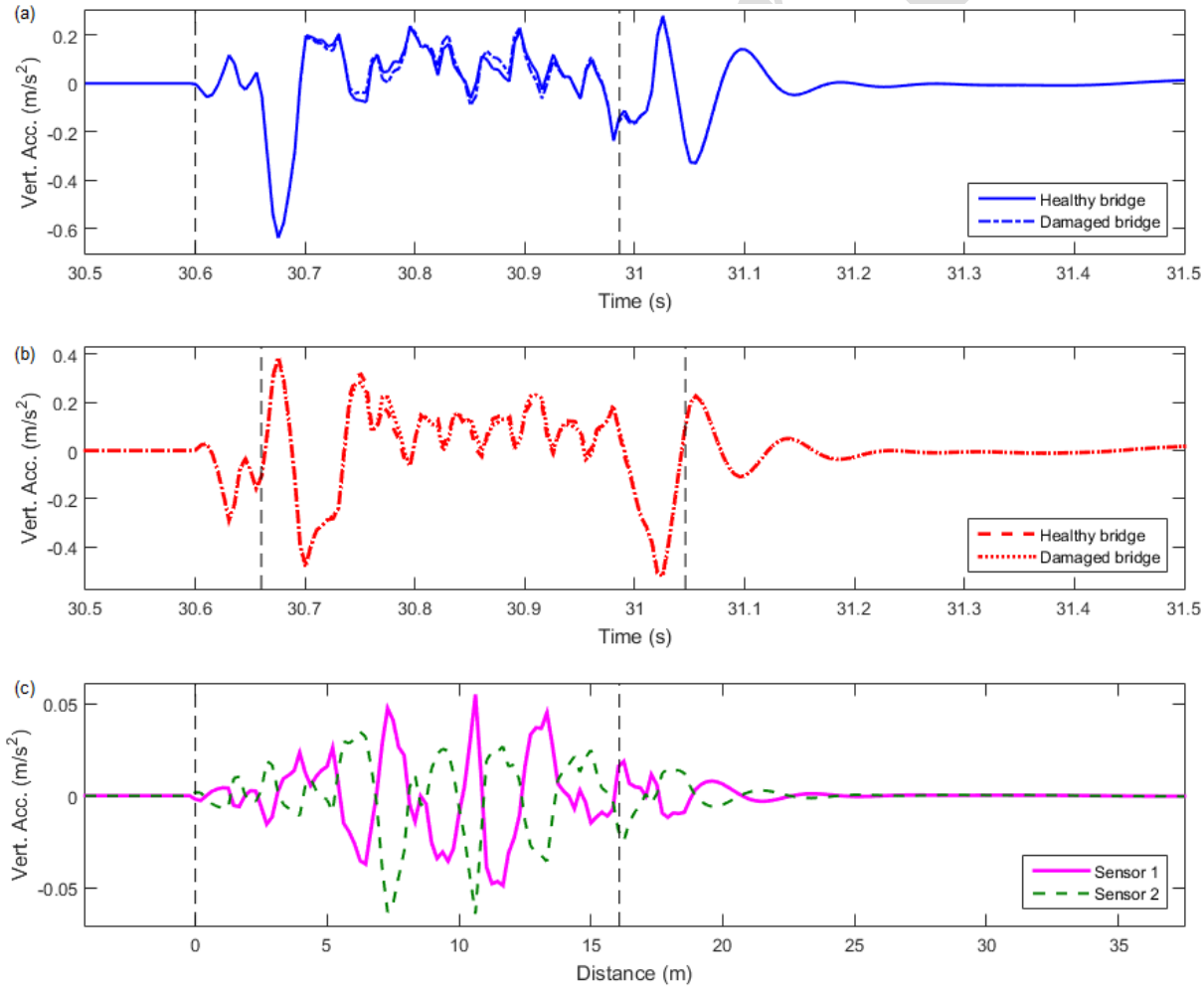

Figure 8. Scenario A: Symmetrical reduction of 0.55 m in bottom flange of mid-span element (7.5% reduction in I_{yy}^t). Input signals generated from 3D interaction model. Vertical dashed lines represent bridge ends. (a) Sensor 1 vertical acceleration; (b) Sensor 2 vertical acceleration; (c) Difference between vertical accelerations for healthy and damaged bridges

The resulting apparent profiles for both healthy and damaged bridges are presented in Figure 9. Figure 9 (a) displays 140 apparent profiles for the healthy bridge scenario; 70 for the 1st axle of the vehicle and 70 for the 2nd axle. The profiles are almost overlapping in the figure which makes them appear as a single thick line at this scale. Figure 9 (b) displays the results of a further 70 simulations for the damaged bridge also resulting in 140 apparent profiles. There is some variance between the profiles due to unavoidable drift associated with the reduced ability of accelerometers to accurately measure low frequency vibration. The long wavelength content of a profile produces very low frequency vibration in the passing vehicle resulting in low frequency, low amplitude readings taken by the sensor. Therefore, in the inverse problem, accuracy of the longer wavelength content in the apparent profiles, inferred from the acceleration signal, is reduced. Repeated simulations using the same input signals will result in apparent profiles with differing magnitudes and directions of drift. The problem of drift is further exacerbated by an accumulation of errors produced by the integration routines in the coupled model solver.

Figure 9 (c) shows the mean of the apparent profiles under both bogie axles for the healthy and damaged bridges. The apparent profile elevations at mid-span for axles 1 and 2 are -1.08 mm and -1.19 mm respectively, providing good agreement with the actual deflection of the bridge at mid-span (1.23 mm). The differences between the actual deflection and the apparent profile elevations can be attributed to the fact that the 2D vehicle model used to infer the profiles is an idealisation of the 3D model and is unable to account for the lateral movements of the vehicle which are excited by the deflection and twisting of the 3D bridge.

It is clear from Figure 9 (c) that there is a small difference between the apparent profiles inferred from the bogie acceleration signals produced by crossing the healthy and damaged bridges. This means that the apparent profiles have the potential to be used as a damage indicator but the sensitivity is poor. The difference between the healthy and damaged apparent profiles, shown in Figure 9 (d), is small and varies over the length of the bridge. The difference at mid-span is not the maximum value and the differences are not the same for both axles. This provides further justification for using the area between zero elevation and the apparent profile over the bridge span as the damage indicator.

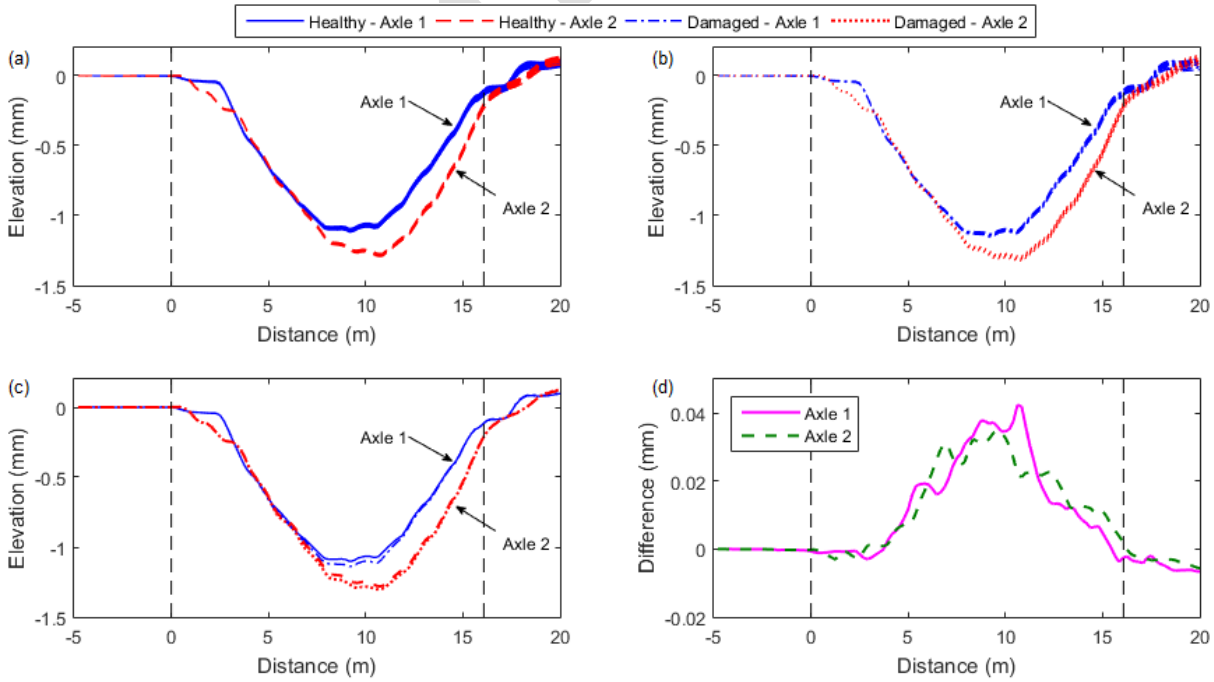

Figure 9. Scenario A: Inferred apparent profiles. Vertical dashed lines represent the bridge ends; (a) 70 apparent profiles for each axle crossing the healthy bridge; (b) 70 apparent profiles for each axle crossing the damaged bridge; (c) Mean apparent profiles; (d) Differences between mean apparent profiles

Due to the differences in the apparent profiles at a given level of damage, it is necessary to use a daily average to prevent outliers from being misinterpreted as an indicator of damage. Figure 10 shows the daily average area between zero elevation and the apparent profile for axle 1. This daily average is calculated as the mean of 5 apparent profiles calculated from the responses of 5 trains crossing the bridge in a day. The bridge is damaged in day 15 and a marked difference in the daily average area is noted. A 7-day moving average is fitted to the daily mean values to indicate that the area between zero elevation and the apparent profile has changed due to the damage. As there are no vertical track irregularities present in this scenario, the apparent profile for the damaged bridge is entirely below the zero elevation. The presence of damage has increased the deflection of the bridge, meaning that an increase in the area is observed.

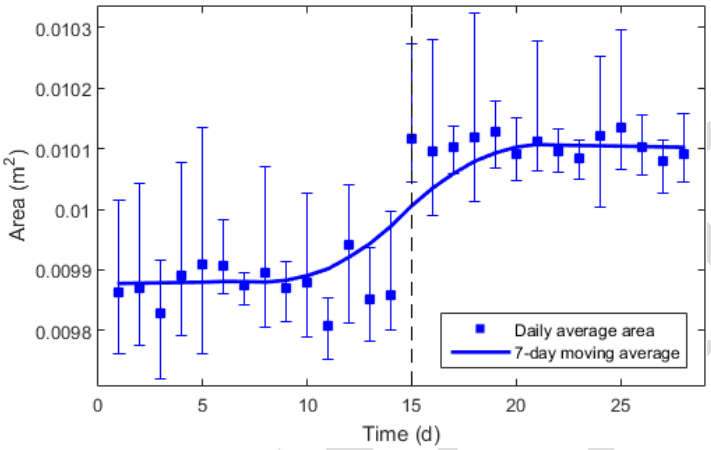

Figure 10. Scenario A: Daily average area under apparent profile (axle 1) between bridge ends (5 passes/day) and 7-day moving average. Vertical bars show range of areas in each day. The vertical dashed line represents the day the bridge was damaged

4.2 Scenario B

In this scenario 'moderate' vertical irregularities generated through the PSD are added to the track. The effect of adding randomly generated sensor noise to the reference signals is also tested. Sensor noise spectra for the range of accelerometers tested are shown in Figure 11. The elevation of the apparent profile produced in this scenario is influenced by the deflection of the bridge, track irregularities, differences in the dynamics between the 3D and 2D vehicles and the effects of sensor noise. Numerical tests using a lower level of damage (Damage Level I) were excessively influenced by the effect of added sensor noise. Therefore results for a higher level of damage (Damage Level II) are presented here.

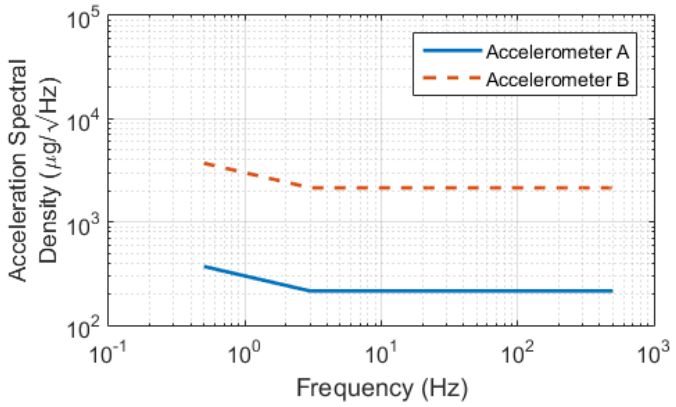

Figure 11. Power Spectral Density for Accelerometers

Figure 12 shows the results of 70 simulations for a healthy bridge and 70 simulations for a damaged bridge with both sensors subject to the noise level for 'Accelerometer A'. It is clear that the effect of noise has increased the variance in the apparent profile elevations and increased the level of drift. The increase in the level of damage has increased the difference (0.17 mm) between the mean profiles as shown in Figure 12 (d). It is also clear from this figure that the measurement of the mid-span elevation of the apparent profile cannot be relied upon to reflect changes in the apparent profile. This confirms that using a measure of the area between zero elevation and the apparent profile over the bridge span is a more reliable method of measuring a change in the apparent profile.

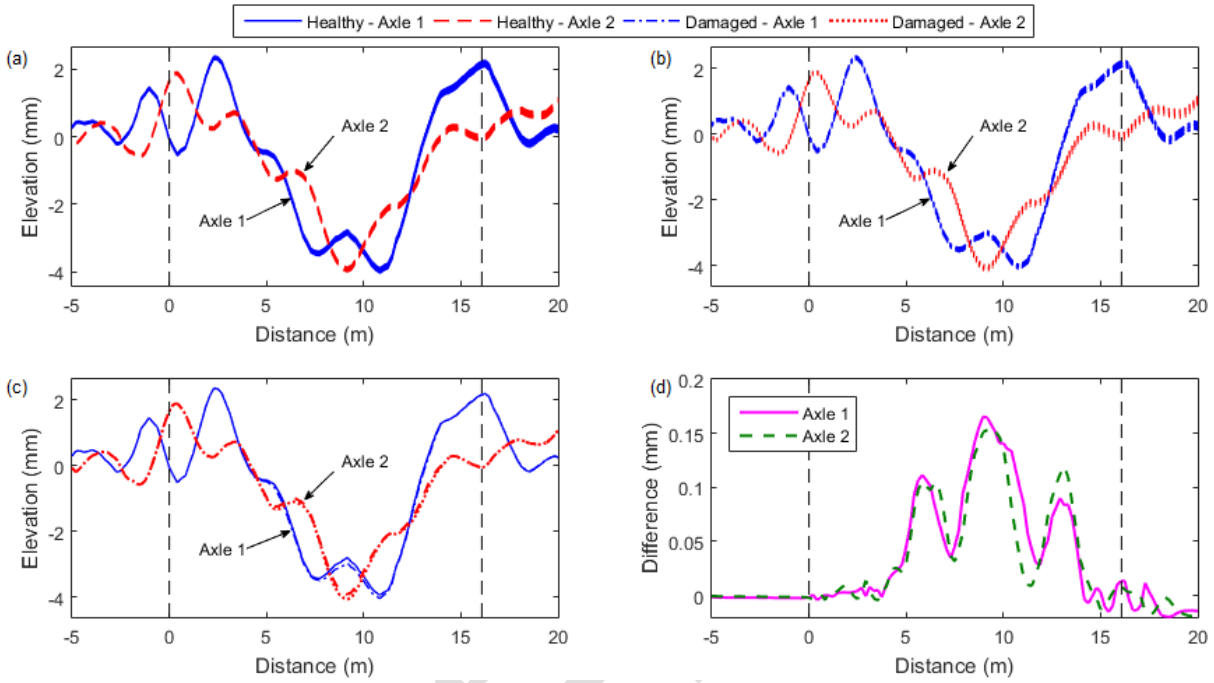

Figure 12. Scenario B: Inferred apparent profiles. Vertical dashed lines represent the bridge ends; (a) 70 apparent profiles for each axle crossing the healthy bridge; (b) 70 apparent profiles for each axle crossing the damaged bridge; (c) Mean apparent profiles; (d) Differences between mean apparent profiles

The trend in the daily average area between zero elevation and the apparent profile for damage scenario B is shown in Figure 13. There is clearly a greater variance in the daily average area for 'Accelerometer B'. However the 7-day moving average still successfully identifies the damage for all levels of noise considered.

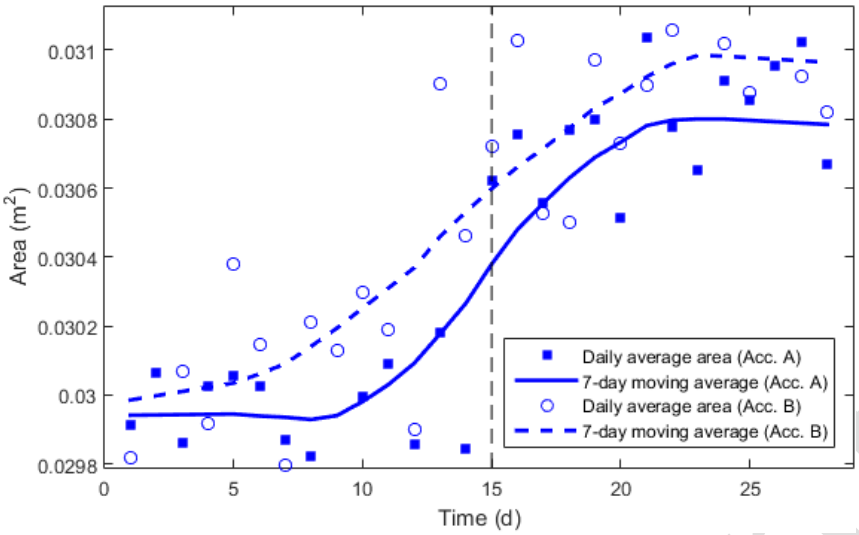

Figure 13. Scenario B: Daily average area under apparent profile (wheel 1) between bridge ends (5 passes/day) and 7-day moving average. The vertical dashed line represents the day damage was applied

4.3 Scenarios B, C & D

In these scenarios the effect of different damage locations is investigated. The same track irregularity profile used in Scenario B is retained so that comparisons to the healthy bridge simulations presented in Scenario B can be made. Figure 14 (a) compares a section of the mean of 70 apparent profiles generated for the healthy bridge to the means of the apparent profiles generated for 3 different damage scenarios, B, C and D, based on 70 apparent profiles for each scenario. The apparent profile for damage scenario D can be observed independently between 7-7.5 m however it overlaps with damage scenario C between 8-10 m. Figure 14 (b) shows the differences between the apparent profiles for healthy and damaged bridges across the bridge span. Damage scenario B has the largest difference. In all scenarios, the peak difference between the healthy and damaged profiles corresponds approximately to the damage location, suggesting that the method has the potential to locate damage. There are three distinct peaks in the graph. The frequency of spacing between the 2nd and 3rd peaks is approximately 10.52 Hz, which matches the eigenfrequency of the bogie pitch found by modal analysis of the vehicle.

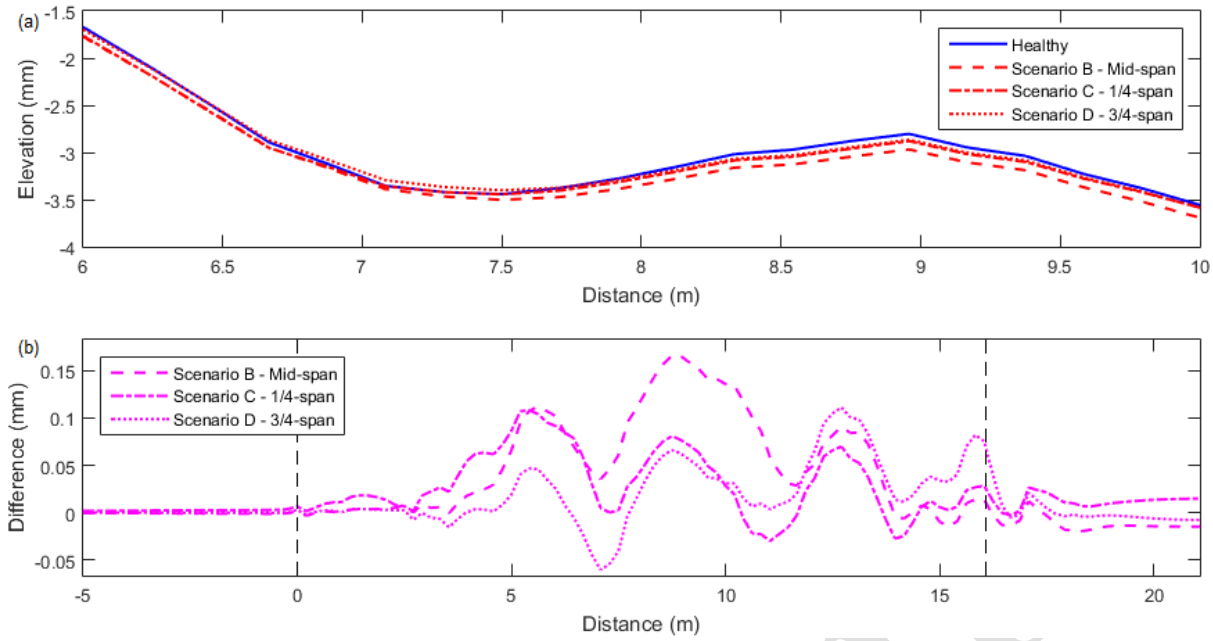

Figure 14. Scenarios B, C & D. (a) Comparison of mean apparent profiles under axle 1 for healthy and damaged bridges with varying damage location (Mid-span area (6 m – 10 m) shown for clarity); (b) Difference between healthy and damaged apparent profiles

It is clear from the differences presented in Figure 14 (b) that the damage indicator, the area between the zero elevation and the apparent profile, is larger for Scenario B. Table 6 lists the areas computed from the mean apparent profile for each scenario. The percentage change in area for Scenario D is only 0.3% demonstrating that it is more difficult to detect damage if it is located at the side of the bridge that the vehicle is exiting. However, most bridges are bi-directional and therefore a train travelling in the opposite direction is more likely to detect damage on this side.

Table 6. Scenario B, C and D. Area between zero elevation and mean apparent profile.

Damage Scenario	Damage Location	Area (m^2)	% Change in Area
Healthy	-	0.03	-
B	Mid-span	0.0307	2.3 %
C	¼ span	0.0304	1.3 %
D	¾ span	0.0301	0.3 %

Figure 15 shows the 7-day moving average of the daily average area (computed for 5 train passes per day) for Scenarios B, C and D with two levels of sensor noise, presented in Figure 11, considered for each scenario. The healthy bridge simulations used in Figure 13 are shuffled so that they are considered on different days in the weekly trend graph. While more simulations are required to provide a more accurate analysis on the tolerance of the method to varying damage location, considering these three damage locations allows us to hypothesise that the method is capable of detecting damage in a bridge where the damage is located between the quarter span and the mid-span. The method is not as effective when damage is located beyond mid-span (Scenario D).

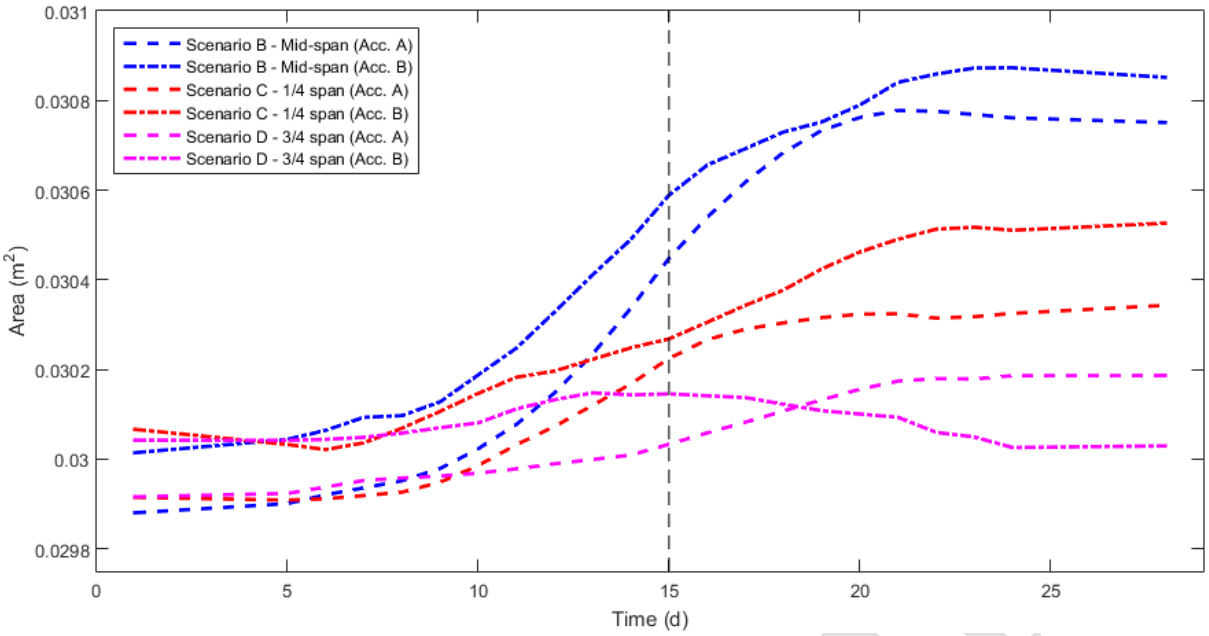

Figure 15. Scenarios B, C & D. 7-day moving average of daily average area under apparent profile (axle 1) between bridge ends (5 passes/day). The vertical dashed line represents the day damage was applied

5.0 DISCUSSION

The bridge damage detection method presented in the previous section has the potential to identify changes in the dynamic behaviour of bridges due to damage. The method uses the measured response of a crossing vehicle to identify an apparent profile which is compared with corresponding historical profiles to detect damage. There are many challenges to be overcome prior to application using actual data measured from an in-service train. A simplified 2D model is used to prove the concept; however, it is acknowledged that an improved model may be required to account for non-linearities in the vehicle suspension system, changes in vehicle mass due to variance in passenger and fuel loading, and temperature effects. It is not yet known how such a model would affect the accuracy of the method and this requires further investigation.

From the numerical analysis the method successfully identifies damage for a signal-to-noise ratio of approximately 60 meaning that high quality, low noise level accelerometers are required in the data acquisition system. In addition, the 2D model used to infer profiles from measured vehicle response is influenced by errors in the vertical acceleration caused by 3D effects such as the pitch and roll of the bogie. The cross-axis sensitivity of the accelerometer used must be as low as possible to minimise these effects. Alternatively, the use of a 3D model to infer profiles would account for some of these issues; however this would increase the model complexity and the computational effort required by the method.

The optimisation method uses an idealised 2D multi-body vehicle model to compare to a reference signal. Methods using numerical models to accurately simulate the response of railway vehicles require knowledge of the geometrical and mechanical properties of the vehicle which can be difficult to obtain from manufacturers [38]. Before this method can be applied to field data, calibration of the vehicle model is required. Damage to the wheels of the vehicle, in the form of wheel flats or wheel out-of-roundness, can have a significant effect on the measured bogie vertical acceleration, and hence the inferred apparent profile. The frequency of the wheel damage is directly proportional to the vehicle velocity, thereby allowing identification of poor quality measurement through analysis of any inconsistencies in the frequency spectrum of the signal. If a significant peak related to a wheel defect is consistently identified, it can be filtered out. Alternatively, instrumentation of multiple bogies on multiple trains allows poor quality measured signals caused by defects to be discarded until the wheel defects are rectified, thereby offering some redundancy in the bridge monitoring system.

The methodology and results presented in the paper demonstrate the capability of the bridge damage detection method through numerical methods. As a result, the influence of a number of factors are not investigated here and could be subject to further work. In theory, since the dynamics of the train are considered in the optimisation technique the method should return the same profile for any speed. The use of a dynamic rigid-body vehicle model to infer profiles allows for the vehicle forward velocity to be varied, and therefore theoretically accounts for changes in the response of the vehicle at different speeds. A constant vehicle forward velocity is used in this paper to prove the concept. However, since the vehicle dynamics are modelled, it is not envisaged that changes in vehicle speed will significantly affect the returned inferred profiles, provided that the forward velocity is accurately measured.

6.0 SUMMARY AND CONCLUSIONS

Daily monitoring using sensors attached to in-service trains has the potential to identify changes to bridge assets. Over time, comparison of apparent profiles should indicate gradual deterioration of the bridge or detect sudden 'impact events' such as bridge strikes empowering railway infrastructure managers to make more informed decisions regarding bridge maintenance. A method for detecting railway bridge damage using comparison of apparent profiles is presented in this paper. An apparent profile is a vertical longitudinal profile which, when applied to an infinitely stiff track model generates the same inertial response in the passing vehicle to that of a bridge crossing. The presence of damage in a bridge changes its stiffness and hence its influence on the passing vehicle. A change in the deflection of the bridge due to damage will manifest itself as a change in the apparent profile which can potentially be used to detect the damage.

The apparent profiles are found using the Cross Entropy combinatorial optimisation method which takes vehicle vertical acceleration signals measured on the bogie above both axles as input. These inputs are generated using a 3D train-bridge interaction model. A 2D car vehicle model is used to find the apparent profile in the optimisation algorithm. Two apparent profiles are inferred for each crossing event due to differences in the deflection of the bridge under the two axles at corresponding locations. Profiles inferred under axle 1 are used to determine the damage indicator, calculated as the area between zero elevation and the apparent profile across the bridge span.

A range of damage scenarios are tested, yielding positive results. Apparent profiles inferred from 5 train passes per day are averaged to remove the effect of the inherent variabilities in the method. A 7-day moving average filter is fitted to the daily average areas for a duration of 4 weeks. This demonstrates how the method might function in a daily monitoring application. The method successfully detects bridge damage in the presence of track irregularity and sensor noise. Damage is detected along a significant portion of the bridge, considering the analysis of bi-directional traffic, however the effectiveness of the method reduces for damage located closer to the supports. On a bi-directional line the damage would be more likely to be detected by a train crossing in an opposite direction.

From the results shown in this paper, it is found that comparison of the apparent profile for bridge crossing events can be used to detect damage in bridges. As a by-product of trains in regular service, this 'drive-by' monitoring technique can be used by railway infrastructure managers to assess the performance of their railway bridges on a regular basis. Performance assessment of railway bridges is needed to evaluate functionality, forecast deterioration and update future inspection and maintenance plans for bridge assets [6].

ACKNOWLEDGEMENT

The research presented in this paper was carried out as part of the Marie Curie Initial Training Network (ITN) action FP7-PEOPLE-2013-ITN.The project has received funding from the European Union's Seventh Framework Programme for research, technological development and demonstration under grant agreement number 607524. The authors are thankful for this support.

REFERENCES

[1] Ward CP, Weston PF, Stewart EJC, Li H, Goodall RM, Roberts C, et al. Condition monitoring opportunities using vehicle-based sensors. Proc Inst Mech Eng Part F J Rail Rapid Transit

2011;225:202–18. doi:10.1177/09544097JRRT406.

[2] Weston P, Roberts C, Yeo G, Stewart E. Perspectives on railway track geometry condition monitoring from in-service railway vehicles. Veh Syst Dyn Int J Veh Mech Mobil 2015;53:1063–91. doi:10.1080/00423114.2015.1034730.

[3] Malahide Viaduct - Reinstatement. J Irish Railw Rec Soc 2010;24:2–3.

[4] http://www.irishrail.ie/news/bridgestrikes. Date accessed: 2016-09-06 n.d.

[5] http://www.networkrail.co.uk/aspx/3563.aspx. Date accessed: 2016-11-09 n.d.

[6] Fujino Y, Siringoringo DM. Bridge monitoring in Japan: the needs and strategies. Struct Infrastruct Eng 2011;7:597–611. doi:10.1080/15732479.2010.498282.

[7] Malekjafarian A, McGetrick PJ, OBrien EJ. A Review of Indirect Bridge Monitoring Using Passing Vehicles. Shock Vib 2014;2015.

[8] Doebling SW, Farrar CR, Prime MB. A Summary Review of Vibration-Based Damage Identification Methods. Shock Vib Dig 1998;30:91–105. doi:10.1177/058310249803000201.

[9] Alvandi A, Cremona C. Assessment of vibration-based damage identification techniques. J Sound Vib 2006;292:179–202. doi:10.1016/j.jsv.2005.07.036.

[10] Yang Y-B, Lin CW, Yau JD. Extracting bridge frequencies from the dynamic response of a passing vehicle. J Sound Vib 2004;272:471–93. doi:10.1016/S0022-460X(03)00378-X.

[11] Yang YB, Lin CW. Vehicle–bridge interaction dynamics and potential applications. J Sound Vib 2005;284:205–26. doi:10.1016/j.jsv.2004.06.032.

[12] McGetrick PJ. The Use of an Instrumented Vehicle to Monitor Transport Infrastructure. 2012.

[13] Lin CW, Yang YB. Use of a passing vehicle to scan the fundamental bridge frequencies: An experimental verification. Eng Struct 2005;27:1865–78. doi:10.1016/j.engstruct.2005.06.016.

[14] Cantero D, Basu B. Railway infrastructure damage detection using wavelet transformed acceleration reponse of traversing vehicle. Struct Control Heal Monit 2015;22:62–70. doi:10.1002/stc.

[15] IS EN 13848: Railway Applications - Track - Track Geometry Quality - CEN European Committee for Standardisation n.d.

[16] Yang YB, Chang KC. Extracting the bridge frequencies indirectly from a passing vehicle: Parametric study. Eng Struct 2009;31:2448–59. doi:10.1016/j.engstruct.2009.06.001.

[17] EN 1990:2002 - Eurocode - Basis of structural design. 2002.

[18] McGetrick PJ, González A, OBrien EJ. Theoretical investigation of the use of a moving vehicle to identify bridge dynamic parameters. Insight - Non-Destructive Test Cond Monit 2009;51:433–8. doi:10.1784/insi.2009.51.8.433.

[19] He X, Kawatani M, Hayashikawa T, Kim C, Catbas FN, Furuta H. A structural damage detection approach using train-bridge interaction analysis and soft computing methods. Smart Struct Syst 2014;13:869–90.

[20] Shu J, Zhang Z, Gonzalez I, Karoumi R. The application of a damage detection method using Artificial Neural Network and train-induced vibrations on a simplified railway bridge model. Eng Struct 2013;52:408–21. doi:10.1016/j.engstruct.2013.02.031.

[21] OBrien EJ, Keenahan J. Drive-by damage detection in bridges using the apparent profile. Struct Control Heal Monit 2015;22:813–25. doi:10.1002/stc.1721.

[22] Elhattab A, Uddin N, OBrien E. Drive-by bridge damage monitoring using bridge displacement profile difference. J Civ Struct Heal Monit n.d. doi:10.1007/s13349-016-0203-6.

[23] OBrien EJ, Bowe C, Quirke P, Cantero D. Determination of longitudinal profile of railway track using vehicle-based inertial readings. J Rail Rapid Transit 2016;0:1–17. doi:10.1177/0954409716664936.

[24] Dassalt Systems ABAQUS Documentation 2011.

[25] Nguyen K, Goicolea JM, Galbadon F. Comparison of dynamic effects of high-speed traffic load on ballasted track using simplified two-dimensional and full three-dimensional model. Proc Inst Mech Eng Part F J Rail Rapid Transit 2014;228:128–42.

[26] Goicolea Ruigómez JM. Unofficial description of loads and masses of high speed train in Spanish network AVE S-103 (Siemens ICE3 Velaro). Monografía (Technical Report). E.T.S.I. Caminos, Canales Y Puertos (UPM), Madrid: 2014.

[27] Antolín P, Goicolea JM, Oliva J, Astiz M a. Nonlinear Train-Bridge Lateral Interaction Using a Simplified Wheel-Rail Contact Method Within a Finite Element Framework. J Comput Nonlinear Dyn 2012;7:41014. doi:10.1115/1.4006736.

[28] Martínez-Corcoba R. Estudio del comportamiento dinámico y estructural del puente sobre el río Torote frente a las acciones del nuevo tráfico ferroviario [In Spanish]. Proyecto Fin de Carrera / Trabajo Fin de Grado, E.T.S.I. Caminos, Canales y Puertos (UPM), Madrid, 2015.

[29] White RC, Limbert DA, Hederick JK, Cooperrider NK. Guideway-suspension tradeoffs in rail vehicle systems, Report ERC-R-78035. 1978.

[30] Azimi H. Development of VBI models with vehicle acceleration for bridge-vehicle dynamic response. 2011.

[31] Ferrara R. A numerical model to predict train induced vibrations and dynamic overloads. 2013.

[32] Wu YS, Yang Y Bin. Steady-state response and riding comfort of trains moving over a series of simply supported bridges. Eng Struct 2003;25:251–65. doi:10.1016/S0141-0296(02)00147-5.

[33] Cantero D, Arvidsson T, OBrien E, Karoumi R. Train–track–bridge modelling and review of parameters. Struct Infrastruct Eng 2015;2479:1–14. doi:10.1080/15732479.2015.1076854.

[34] Bathe KJ, Wilson EL. Numerical methods in finite element analysis. Englewood Cliffs, UK: Prentice Hall; 1976.

[35] Tedesco JW, McDougal WG, Ross CA. Structural dynamics, theory and applications. California, USA: Addison Wesley Longman; 1999.

[36] MathWorks. Matlab 2016.

[37] Weaver W, Johnston PR. Structural dynamics by finite elements. Harlow, UK: Prentice Hall; 1987.

[38] Ribeiro D, Calçada R, Delgado R, Brehm M, Zabel V. Finite-element model calibration of a railway vehicle based on experimental modal parameters. Veh Syst Dyn 2013;51:821–56. doi:10.1080/00423114.2013.778416.

APPENDIX A

Irregularity profile used in Damage Scenarios B, C and D.

s (m)	z (mm)		s (m)	z (mm)		s (m)	z (mm)
-10.000	0.000		4.971	-1.210		20.312	1.320
-9.616	0.013		5.355	-1.250		20.696	1.270
-9.232	0.026		5.738	-1.210		21.080	1.080
-8.849	0.037		6.122	-1.200		21.463	0.964
-8.465	0.051		6.505	-1.290		21.847	0.884
-8.082	0.064		6.889	-1.520		22.230	0.803
-7.698	0.077		7.272	-1.890		22.614	0.723
-7.315	0.090		7.656	-2.340		22.997	0.643
-6.931	0.103		8.040	-2.750		23.381	0.562
-6.548	0.116		8.423	-3.040		23.764	0.482
-6.164	0.129		8.807	-3.130		24.148	0.402
-5.781	0.141		9.190	-2.980		24.531	0.321
-5.397	0.200		9.574	-2.610		24.915	0.241
-5.014	0.250		9.957	-2.060		25.298	0.161
-5.000	0.260		10.341	-1.420		25.682	0.080
-4.616	0.398		10.724	-0.737		26.065	0.000
-4.232	0.621		11.108	-0.078			
-3.849	0.706		11.491	0.532			
-3.465	0.582		11.875	1.090			
-3.082	0.280		12.258	1.600			
-2.698	-0.080		12.642	2.050			
-2.315	-0.340		13.025	2.420			
-1.931	-0.366		13.409	2.660			
-1.548	-0.107		13.792	2.730			
-1.164	0.386		14.176	2.610			
-0.781	0.984		14.560	2.300			
-0.397	1.530		14.943	1.860			
-0.014	1.910		15.327	1.350			
0.369	2.070		15.710	0.864			
0.752	2.040		16.094	0.445			
1.136	1.900		16.477	0.118			
1.520	1.700		16.861	-0.127			
1.903	1.500		17.244	-0.308			
2.287	1.280		17.628	-0.426			
2.670	1.010		18.011	-0.460			
3.054	0.653		18.395	-0.369			
3.437	0.213		18.778	-0.124			
3.821	-0.263		19.162	0.260			
4.204	-0.702		19.545	0.710			
4.588	-1.030		19.929	1.100			

APPENDIX B

Vertical acceleration signals generated in 3D interaction model for each damage scenario.

	A		B		C		D	
t	$\ddot{u}_1$	$\ddot{u}_2$	$\ddot{u}_1$	$\ddot{u}_2$	$\ddot{u}_1$	$\ddot{u}_2$	$\ddot{u}_1$	$\ddot{u}_2$
(s)	$(m/s)^2$	$(m/s)^2$	$(m/s)^2$	$(m/s)^2$	$(m/s)^2$	$(m/s)^2$	$(m/s)^2$	$(m/s)^2$
30.480	-0.00001	0.00003	0.00261	0.00347	0.00261	0.00347	0.00261	0.00347
30.485	0.00000	0.00003	0.00213	0.00350	0.00213	0.00350	0.00213	0.00350
30.490	0.00000	0.00003	0.00163	0.00320	0.00163	0.00320	0.00163	0.00320
30.495	0.00001	0.00004	0.00117	0.00263	0.00117	0.00263	0.00117	0.00263
30.500	0.00001	0.00004	0.00078	0.00188	0.00078	0.00188	0.00078	0.00188
30.505	0.00001	0.00005	0.00044	0.00105	0.00044	0.00105	0.00044	0.00105
30.510	0.00002	0.00005	0.00013	0.00020	0.00013	0.00020	0.00013	0.00020
30.515	0.00002	0.00005	-0.00017	-0.00059	-0.00017	-0.00059	-0.00017	-0.00059
30.520	0.00002	0.00006	-0.00046	-0.00127	-0.00046	-0.00127	-0.00046	-0.00127
30.525	0.00003	0.00006	-0.00075	-0.00181	-0.00075	-0.00181	-0.00075	-0.00181
30.530	0.00003	0.00007	-0.00104	-0.00218	-0.00104	-0.00218	-0.00104	-0.00218
30.535	0.00004	0.00007	-0.00130	-0.00240	-0.00130	-0.00240	-0.00130	-0.00240
30.540	0.00004	0.00008	-0.00154	-0.00248	-0.00154	-0.00248	-0.00154	-0.00248
30.545	0.00005	0.00008	-0.00173	-0.00243	-0.00173	-0.00243	-0.00173	-0.00243
30.550	0.00005	0.00008	-0.00186	-0.00229	-0.00186	-0.00229	-0.00186	-0.00229
30.555	0.00005	0.00009	-0.00192	-0.00208	-0.00192	-0.00208	-0.00192	-0.00208
30.560	0.00006	0.00009	-0.00190	-0.00184	-0.00190	-0.00184	-0.00190	-0.00184
30.565	0.00006	0.00010	-0.00181	-0.00158	-0.00181	-0.00158	-0.00181	-0.00158
30.570	0.00007	0.00010	-0.00166	-0.00133	-0.00166	-0.00133	-0.00166	-0.00133
30.575	0.00007	0.00010	-0.00145	-0.00109	-0.00145	-0.00109	-0.00145	-0.00109
30.580	0.00007	0.00011	-0.00121	-0.00088	-0.00121	-0.00088	-0.00121	-0.00088
30.585	0.00008	0.00011	-0.00094	-0.00070	-0.00094	-0.00070	-0.00094	-0.00070
30.590	0.00008	0.00011	-0.00067	-0.00055	-0.00067	-0.00055	-0.00067	-0.00055
30.595	0.00009	0.00012	-0.00041	-0.00043	-0.00041	-0.00043	-0.00041	-0.00043
30.600	-0.00218	0.00236	-0.00017	-0.00033	-0.00017	-0.00033	-0.00017	-0.00033
30.605	-0.02859	0.02268	0.00002	-0.00025	0.00002	-0.00025	0.00002	-0.00025
30.610	-0.05624	0.02780	0.00017	-0.00018	0.00017	-0.00018	0.00017	-0.00018
30.615	-0.04816	-0.01266	0.00027	-0.00013	0.00027	-0.00013	0.00027	-0.00013
30.620	-0.00950	-0.08492	0.00032	-0.00009	0.00032	-0.00009	0.00032	-0.00009
30.625	0.04750	-0.17822	0.00033	-0.00006	0.00033	-0.00006	0.00033	-0.00006
30.630	0.11338	-0.28341	0.00031	-0.00004	0.00031	-0.00004	0.00031	-0.00004
30.635	0.08698	-0.23172	0.00025	-0.00004	0.00025	-0.00004	0.00025	-0.00004
30.640	0.00082	-0.08206	0.00017	-0.00005	0.00017	-0.00005	0.00017	-0.00005
30.645	-0.02602	-0.03535	0.00008	-0.00007	0.00008	-0.00007	0.00008	-0.00007
30.650	0.00303	-0.08507	-0.00001	-0.00010	-0.00001	-0.00010	-0.00001	-0.00010
30.655	0.04322	-0.15812	-0.00011	-0.00015	-0.00011	-0.00015	-0.00011	-0.00015
30.660	-0.04764	-0.10311	-0.00019	-0.00020	-0.00019	-0.00020	-0.00019	-0.00020
30.665	-0.28715	0.06133	-0.00027	-0.00025	-0.00027	-0.00025	-0.00027	-0.00025
30.670	-0.53434	0.29182	-0.00034	-0.00030	-0.00034	-0.00030	-0.00034	-0.00030
30.675	-0.64028	0.38623	-0.00039	-0.00035	-0.00039	-0.00035	-0.00039	-0.00035
30.680	-0.58042	0.29180	-0.00043	-0.00040	-0.00043	-0.00040	-0.00043	-0.00040
30.685	-0.44773	0.11101	-0.00045	-0.00044	-0.00045	-0.00044	-0.00045	-0.00044
30.690	-0.28952	-0.10880	-0.00047	-0.00046	-0.00047	-0.00046	-0.00047	-0.00046
30.695	-0.00577	-0.39271	-0.00047	-0.00048	-0.00047	-0.00048	-0.00047	-0.00048
30.700	0.18605	-0.48288	-0.00047	-0.00049	-0.00047	-0.00049	-0.00047	-0.00049
30.705	0.18752	-0.39300	-0.00046	-0.00048	-0.00046	-0.00048	-0.00046	-0.00048
30.710	0.16829	-0.33128	-0.00044	-0.00047	-0.00044	-0.00047	-0.00044	-0.00047
30.715	0.16576	-0.31185	-0.00041	-0.00045	-0.00041	-0.00045	-0.00041	-0.00045
30.720	0.13852	-0.28535	-0.00039	-0.00042	-0.00039	-0.00042	-0.00039	-0.00042

		A			B			C			D	
t		$\ddot{u}_1$	$\ddot{u}_2$		$\ddot{u}_1$	$\ddot{u}_2$		$\ddot{u}_1$	$\ddot{u}_2$		$\ddot{u}_1$	$\ddot{u}_2$
(s)		$(m/s)^2$	$(m/s)^2$		$(m/s)^2$	$(m/s)^2$		$(m/s)^2$	$(m/s)^2$		$(m/s)^2$	$(m/s)^2$
30.725		0.13553	-0.27287		-0.00036	-0.00039		-0.00036	-0.00039		-0.00036	-0.00039
30.730		0.19852	-0.23901		-0.00033	-0.00035		-0.00033	-0.00035		-0.00033	-0.00035
30.735		0.10796	-0.01526		-0.00030	-0.00032		-0.00030	-0.00032		-0.00030	-0.00032
30.740		-0.01828	0.19914		-0.00027	-0.00028		-0.00027	-0.00028		-0.00027	-0.00028
30.745		-0.04089	0.27456		-0.00024	-0.00025		-0.00024	-0.00025		-0.00024	-0.00025
30.750		-0.03572	0.28177		-0.00022	-0.00022		-0.00022	-0.00022		-0.00022	-0.00022
30.755		-0.03996	0.24295		-0.00019	-0.00020		-0.00019	-0.00020		-0.00019	-0.00020
30.760		0.09665	0.08026		-0.00017	-0.00018		-0.00017	-0.00018		-0.00017	-0.00018
30.765		0.11949	0.10213		-0.00016	-0.00016		-0.00016	-0.00016		-0.00016	-0.00016
30.770		0.01724	0.22206		-0.00014	-0.00015		-0.00014	-0.00015		-0.00014	-0.00015
30.775		0.00344	0.22071		-0.00013	-0.00014		-0.00013	-0.00014		-0.00013	-0.00014
30.780		0.05008	0.14793		-0.00013	-0.00014		-0.00013	-0.00014		-0.00013	-0.00014
30.785		0.06171	0.08611		-0.00012	-0.00014		-0.00012	-0.00014		-0.00012	-0.00014
30.790		0.12189	-0.00948		-0.00012	-0.00013		-0.00012	-0.00013		-0.00012	-0.00013
30.795		0.23739	-0.06523		-0.00013	-0.00013		-0.00013	-0.00013		-0.00013	-0.00013
30.800		0.20933	0.05146		-0.00013	-0.00013		-0.00013	-0.00013		-0.00013	-0.00013
30.805		0.15086	0.14817		-0.00013	-0.00014		-0.00013	-0.00014		-0.00013	-0.00014
30.810		0.15897	0.13596		-0.00014	-0.00014		-0.00014	-0.00014		-0.00014	-0.00014
30.815		0.14188	0.10935		-0.00014	-0.00014		-0.00014	-0.00014		-0.00014	-0.00014
30.820		0.06750	0.10758		-0.00015	-0.00014		-0.00015	-0.00014		-0.00015	-0.00014
30.825		0.17403	-0.00103		-0.00015	-0.00014		-0.00015	-0.00014		-0.00015	-0.00014
30.830		0.19974	0.04422		0.07751	-0.07649		0.07751	-0.07649		0.07751	-0.07649
30.835		0.10042	0.15021		0.07673	-0.05947		0.07673	-0.05947		0.07673	-0.05947
30.840		0.04720	0.14919		0.03157	-0.00247		0.03157	-0.00247		0.03157	-0.00247
30.845		0.00246	0.12045		-0.00312	0.03686		-0.00312	0.03686		-0.00312	0.03686
30.850		-0.09105	0.13143		-0.02974	0.06588		-0.02974	0.06588		-0.02974	0.06588
30.855		-0.05346	0.06845		-0.04650	0.08304		-0.04650	0.08304		-0.04650	0.08304
30.860		0.10154	-0.00146		-0.05327	0.08838		-0.05327	0.08838		-0.05327	0.08838
30.865		0.13595	0.05001		-0.05113	0.08330		-0.05113	0.08330		-0.05113	0.08330
30.870		0.10902	0.10691		-0.04208	0.07018		-0.04208	0.07018		-0.04208	0.07018
30.875		0.10394	0.11666		-0.02864	0.05190		-0.02864	0.05190		-0.02864	0.05190
30.880		0.07610	0.13021		-0.01339	0.03146		-0.01339	0.03146		-0.01339	0.03146
30.885		0.03913	0.13234		0.00131	0.01156		0.00131	0.01156		0.00131	0.01156
30.890		0.19593	0.00768		0.09492	-0.08565		0.09492	-0.08565		0.09492	-0.08565
30.895		0.23052	0.04079		0.15091	-0.12969		0.15091	-0.12969		0.15091	-0.12969
30.900		0.11314	0.17490		0.13838	-0.10876		0.13838	-0.10876		0.13838	-0.10876
30.905		0.04875	0.22703		0.10372	-0.07193		0.10372	-0.07193		0.10372	-0.07193
30.910		0.00940	0.22974		0.06374	-0.03105		0.06374	-0.03105		0.06374	-0.03105
30.915		-0.06287	0.21658		0.02465	0.00771		0.02465	0.00771		0.02465	0.00771
30.920		0.00008	0.08071		-0.00908	0.03989		-0.00908	0.03989		-0.00908	0.03989
30.925		0.09289	0.00027		-0.03451	0.06264		-0.03451	0.06264		-0.03451	0.06264
30.930		0.05987	0.06221		-0.05023	0.07474		-0.05023	0.07474		-0.05023	0.07474
30.935		0.02491	0.11134		0.17467	-0.10660		0.17467	-0.10660		0.17467	-0.10660
30.940		0.02788	0.10487		0.19401	-0.08457		0.19401	-0.08457		0.19401	-0.08457
30.945		-0.01646	0.09875		0.03134	0.08424		0.03134	0.08424		0.03134	0.08424
30.950		-0.06499	0.07321		1.29058	-1.18108		1.29058	-1.18108		1.29058	-1.18108
30.955		0.05819	-0.03680		1.55083	-1.48575		1.55083	-1.48575		1.55083	-1.48575
30.960		0.11038	-0.01429		-0.26700	0.65446		-0.26700	0.65446		-0.26700	0.65446
30.965		0.04965	0.07563		-1.07120	1.50598		-1.07120	1.50598		-1.07120	1.50598
30.970		0.00179	0.10159		-0.82518	1.43582		-0.82518	1.43582		-0.82518	1.43582
30.975		-0.08266	0.12757		-0.65779	1.29034		-0.65779	1.29034		-0.65779	1.29034
30.980		-0.23055	0.18860		-1.01428	1.15193		-1.01428	1.15193		-1.01428	1.15193

	A		B		C		D	
t	$\ddot{u}_1$	$\ddot{u}_2$	$\ddot{u}_1$	$\ddot{u}_2$	$\ddot{u}_1$	$\ddot{u}_2$	$\ddot{u}_1$	$\ddot{u}_2$
(s)	$(m/s)^2$	$(m/s)^2$	$(m/s)^2$	$(m/s)^2$	$(m/s)^2$	$(m/s)^2$	$(m/s)^2$	$(m/s)^2$
30.985	-0.15734	0.08918	-1.09120	1.11283	-1.09120	1.11283	-1.09120	1.11283
30.990	-0.13135	0.00049	-1.31449	0.66452	-1.31449	0.66452	-1.31449	0.66452
30.995	-0.16424	-0.08597	-0.77206	0.01194	-0.77206	0.01194	-0.77206	0.01194
31.000	-0.16598	-0.18649	-0.43743	-0.82754	-0.43743	-0.82754	-0.43743	-0.82754
31.005	-0.13501	-0.27261	-0.41554	-1.07369	-0.41554	-1.07369	-0.41554	-1.07369
31.010	-0.11613	-0.31779	1.43283	-2.84412	1.43283	-2.84412	1.43283	-2.84412
31.015	-0.03462	-0.37914	2.60649	-3.74048	2.60649	-3.74048	2.60649	-3.74048
31.020	0.19462	-0.50821	2.35189	-2.99368	2.35189	-2.99368	2.35189	-2.99368
31.025	0.28299	-0.52211	2.40304	-2.21779	2.40304	-2.21779	2.40304	-2.21779
31.030	0.18229	-0.39810	3.05599	-2.36684	3.05599	-2.36684	3.05599	-2.36684
31.035	0.04649	-0.24182	3.15197	-1.44868	3.15197	-1.44868	3.15197	-1.44868
31.040	-0.09104	-0.07764	0.44783	1.12255	0.44783	1.12255	0.44783	1.12255
31.045	-0.23251	0.08438	-0.67691	2.93561	-0.67691	2.93561	-0.67691	2.93561
31.050	-0.32614	0.19636	-3.78934	5.57486	-3.78934	5.57486	-3.78934	5.57486
31.055	-0.33125	0.22615	-4.61547	6.47533	-4.61547	6.47533	-4.61547	6.47533
31.060	-0.28351	0.20495	-6.43101	7.54369	-6.43101	7.54369	-6.43101	7.54369
31.065	-0.21256	0.15848	-6.67262	7.22648	-6.67262	7.22648	-6.67262	7.22648
31.070	-0.13041	0.09814	-5.52049	5.43841	-5.52143	5.43934	-5.52047	5.43838
31.075	-0.04809	0.03470	-2.86597	2.61391	-2.86900	2.61728	-2.86586	2.61381
31.080	0.02530	-0.02283	-0.35834	-0.64607	-0.35630	-0.64981	-0.35841	-0.64597
31.085	0.08320	-0.06789	4.01188	-4.81507	4.01512	-4.82855	4.01186	-4.81494
31.090	0.12194	-0.09675	5.36688	-6.62087	5.35840	-6.62722	5.36711	-6.62069
31.095	0.14067	-0.10842	8.45323	-9.23072	8.43369	-9.21744	8.45336	-9.22972
31.100	0.14095	-0.10430	8.45742	-9.30468	8.43337	-9.28036	8.45748	-9.30237
31.105	0.12611	-0.08758	8.92432	-9.10378	8.91087	-9.09966	8.92432	-9.09990
31.110	0.10063	-0.06247	7.04258	-6.95332	7.05381	-6.98864	7.04309	-6.94986
31.115	0.06933	-0.03357	5.10485	-4.58485	5.13673	-4.64640	5.10685	-4.58370
31.120	0.03679	-0.00517	2.00594	-1.33366	2.05047	-1.40328	2.00767	-1.32988
31.125	0.00685	0.01922	-0.88034	1.56438	-0.82740	1.49452	-0.88278	1.57846
31.130	-0.01770	0.03713	-4.87849	5.15641	-4.80007	5.06341	-4.87565	5.16992
31.135	-0.03521	0.04731	-7.36029	7.24071	-7.29633	7.15472	-7.34099	7.23813
31.140	-0.04520	0.04966	-9.22129	8.34879	-9.23880	8.34698	-9.19694	8.33533
31.145	-0.04816	0.04506	-9.17322	7.80566	-9.28128	7.90765	-9.15457	7.79238
31.150	-0.04530	0.03508	-9.28405	7.28725	-9.44416	7.47059	-9.27273	7.28347
31.155	-0.03828	0.02168	-7.39557	4.84941	-7.53397	5.03643	-7.39163	4.86169
31.160	-0.02892	0.00691	-4.87904	1.87458	-4.97459	2.01573	-4.88009	1.89803
31.165	-0.01896	-0.00734	-1.95992	-1.20046	-2.02957	-1.12027	-1.96285	-1.18077
31.170	-0.00983	-0.01957	0.34870	-3.44938	0.31488	-3.43478	0.34621	-3.44427
31.175	-0.00257	-0.02872	2.28941	-5.01891	2.30674	-5.05162	2.28997	-5.02273
31.180	0.00225	-0.03430	4.34482	-6.45804	4.41414	-6.51326	4.35505	-6.46073
31.185	0.00449	-0.03627	5.12858	-6.85834	5.23636	-6.91931	5.15519	-6.85736
31.190	0.00436	-0.03506	5.36932	-6.45423	5.48578	-6.50899	5.41062	-6.44993
31.195	0.00236	-0.03135	4.51856	-5.25170	4.63456	-5.30625	4.56250	-5.24328
31.200	-0.00087	-0.02601	3.01460	-3.07735	3.15272	-3.14761	3.05034	-3.06343
31.205	-0.00462	-0.01992	0.68299	-0.31876	0.82253	-0.37388	0.69809	-0.28307
31.210	-0.00827	-0.01389	-0.93954	1.82436	-0.85816	1.84366	-0.95090	1.89760
31.215	-0.01131	-0.00858	-2.69350	3.74423	-2.69197	3.85131	-2.71956	3.84481
31.220	-0.01339	-0.00444	-3.59245	4.65598	-3.67305	4.83647	-3.63603	4.77537
31.225	-0.01435	-0.00169	-3.55847	4.57476	-3.73532	4.82595	-3.63642	4.71506
31.230	-0.01423	-0.00036	-3.27480	3.99916	-3.45299	4.23501	-3.35038	4.11447
31.235	-0.01316	-0.00028	-2.79564	3.36301	-2.81264	3.40778	-2.78054	3.34508
31.240	-0.01139	-0.00119	-0.72449	1.48129	-0.58151	1.33961	-0.61700	1.33640

		A			B			C			D	
t		$\ddot{u}_1$	$\ddot{u}_2$		$\ddot{u}_1$	$\ddot{u}_2$		$\ddot{u}_1$	$\ddot{u}_2$		$\ddot{u}_1$	$\ddot{u}_2$
(s)		$(m/s)^2$	$(m/s)^2$		$(m/s)^2$	$(m/s)^2$		$(m/s)^2$	$(m/s)^2$		$(m/s)^2$	$(m/s)^2$
31.245		-0.00922	-0.00272		0.44108	-0.02873		0.64760	-0.25127		0.57466	-0.22445
31.250		-0.00695	-0.00452		2.63989	-2.22894		2.84201	-2.45785		2.74442	-2.41563
31.255		-0.00484	-0.00629		3.98156	-3.82726		4.15083	-4.03759		4.04033	-3.98947
31.260		-0.00312	-0.00779		4.86686	-4.68236		4.97875	-4.85323		4.87365	-4.81218
31.265		-0.00191	-0.00885		5.17574	-4.84908		5.19854	-4.93786		5.12439	-4.92434
31.270		-0.00126	-0.00941		4.77079	-4.27243		4.71288	-4.27747		4.68646	-4.30036
31.275		-0.00115	-0.00946		3.70154	-2.81783		3.58750	-2.75648		3.61227	-2.81625
31.280		-0.00150	-0.00908		1.90112	-1.02951		1.75106	-0.92117		1.81264	-1.00514
31.285		-0.00219	-0.00840		0.65920	0.70896		0.49976	0.83781		0.57471	0.75232
31.290		-0.00309	-0.00757		-0.62740	2.29655		-0.78725	2.43197		-0.71252	2.36281
31.295		-0.00409	-0.00673		-3.23376	4.62406		-3.40054	4.76106		-3.32991	4.71754
31.300		-0.00505	-0.00601		-3.99205	5.84253		-4.12701	5.95532		-4.06927	5.93233
31.305		-0.00589	-0.00550		-5.00395	6.72081		-5.07518	6.77865		-5.04475	6.77767
31.310		-0.00655	-0.00524		-4.73965	6.56960		-4.73037	6.55086		-4.73957	6.58288
31.315		-0.00701	-0.00525		-4.13030	5.75232		-4.05821	5.66609		-4.10117	5.72398
31.320		-0.00728	-0.00552		-3.33412	4.82469		-3.22069	4.68833		-3.28292	4.75931
31.325		-0.00740	-0.00602		-1.36918	2.78472		-1.22101	2.60534		-1.29069	2.67629
31.330		-0.00741	-0.00669		0.16885	1.12637		0.25339	0.98280		0.20931	1.01905
31.335		-0.00738	-0.00748		2.70893	-1.25697		2.66856	-1.31499		2.66788	-1.32387
31.340		-0.00734	-0.00829		3.79087	-2.57274		3.66858	-2.58652		3.69747	-2.61535
31.345		-0.00733	-0.00908		5.80316	-4.36427		5.64373	-4.36305		5.70260	-4.40765
31.350		-0.00738	-0.00977		7.94122	-6.32840		7.77016	-6.31297		7.86130	-6.38355
31.355		-0.00749	-0.01034		6.32610	-5.02170		6.16749	-4.99668		6.27728	-5.09388
31.360		-0.00767	-0.01076		5.87030	-4.23095		5.75980	-4.22598		5.82632	-4.29043
31.365		-0.00790	-0.01103		4.84630	-3.16345		4.80527	-3.19848		4.78360	-3.16245
31.370		-0.00815	-0.01114		4.05355	-2.09211		4.07682	-2.15543		4.01262	-2.06533
31.375		-0.00837	-0.01108		2.05311	-0.11473		2.12424	-0.17975		2.05333	-0.07453
31.380		-0.00854	-0.01087		0.33831	1.67563		0.43702	1.63616		0.37546	1.73726
31.385		-0.00862	-0.01053		-1.29611	3.03686		-1.18874	3.03571		-1.24017	3.12640
31.390		-0.00859	-0.01008		-2.64224	4.14144		-2.54075	4.17648		-2.56954	4.23361
31.395		-0.00845	-0.00955		-2.94672	3.99441		-2.86414	4.05706		-2.85071	4.06667
31.400		-0.00819	-0.00896		-3.18444	3.86824		-3.12940	3.94885		-3.09633	3.94802
31.405		-0.00779	-0.00830		-3.23445	3.14300		-3.20821	3.23612		-3.18894	3.26416
31.410		-0.00724	-0.00757		-3.95344	2.80231		-3.94719	2.89748		-3.92469	2.93709
31.415		-0.00655	-0.00672		-4.06085	2.27438		-4.06085	2.35073		-3.99599	2.34599
31.420		-0.00570	-0.00573		-3.03840	0.49448		-3.03880	0.53356		-2.92421	0.45701
31.425		-0.00471	-0.00456		-1.98395	-1.05445		-1.98954	-1.05516		-1.88393	-1.14465
31.430		-0.00358	-0.00320		-0.66237	-2.65385		-0.66785	-2.68961		-0.63662	-2.70712
31.435		-0.00233	-0.00166		-0.05266	-3.35696		-0.04265	-3.42050		-0.06576	-3.37584
31.440		-0.00100	0.00005		0.69578	-4.12754		0.72871	-4.20657		0.68499	-4.14373
31.445		0.00039	0.00186		0.53613	-3.94075		0.58399	-4.02127		0.51149	-3.94359
31.450		0.00180	0.00371		0.69601	-3.75967		0.73880	-3.82686		0.59996	-3.71110
31.455		0.00319	0.00554		0.33444	-3.19026		0.35599	-3.23199		0.22882	-3.12758
31.460		0.00454	0.00729		-0.42152	-1.79670		-0.43912	-1.79286		-0.41324	-1.81918
31.465		0.00584	0.00893		-1.85250	-0.10068		-1.88215	-0.07029		-1.72058	-0.20989
31.470		0.00708	0.01044		-4.01955	1.93605		-4.04245	1.97925		-3.84149	1.80693
31.475		0.00825	0.01183		-3.59604	2.00591		-3.61967	2.06330		-3.47117	1.92138
31.480		0.00937	0.01312		-3.86755	2.34173		-3.90691	2.41335		-3.83359	2.31346
31.485		0.01043	0.01434		-3.46723	2.29649		-3.52567	2.37415		-3.49294	2.30821
31.490		0.01142	0.01550		-2.93899	1.95999		-3.00166	2.02944		-2.99300	2.01285
31.495		0.01233	0.01659		-1.64486	1.09994		-1.69020	1.14798		-1.72171	1.18669
31.500		0.01314	0.01760		-0.68930	0.29288		-0.70781	0.31369		-0.79739	0.39933

		A			B			C			D	
t		$\ddot{u}_1$	$\ddot{u}_2$		$\ddot{u}_1$	$\ddot{u}_2$		$\ddot{u}_1$	$\ddot{u}_2$		$\ddot{u}_1$	$\ddot{u}_2$
(s)		$(m/s)^2$	$(m/s)^2$		$(m/s)^2$	$(m/s)^2$		$(m/s)^2$	$(m/s)^2$		$(m/s)^2$	$(m/s)^2$
31.505		0.01384	0.01849		0.69764	-0.66487		0.70879	-0.67714		0.58120	-0.56755
31.510		0.01440	0.01922		2.23582	-1.89620		2.28026	-1.94687		2.14901	-1.83891
31.515		0.01481	0.01977		3.22743	-2.35344		3.30489	-2.43794		3.19215	-2.34955
31.520		0.01507	0.02009		4.10689	-2.51902		4.18278	-2.59935		4.09725	-2.53965
31.525		0.01516	0.02017		4.55673	-2.64575		4.61482	-2.70651		4.56229	-2.68046
31.530		0.01510	0.02002		4.04060	-1.76582		4.07905	-1.80573		4.05976	-1.81220
31.535		0.01488	0.01962		3.56172	-1.01488		3.57920	-1.03240		3.58856	-1.06584
31.540		0.01452	0.01901		2.30257	0.37362		2.30072	0.37688		2.33159	0.32447
31.545		0.01402	0.01823		1.35971	1.37749		1.34237	1.39753		1.38623	1.33543
31.550		0.01342	0.01731		-0.14027	2.53389		-0.16811	2.56541		-0.11953	2.50255
31.555		0.01273	0.01630		-0.76204	3.00388		-0.79489	3.04101		-0.74882	2.98498
31.560		0.01197	0.01524		-1.86294	3.26198		-1.89570	3.29915		-1.85755	3.25550
31.565		0.01116	0.01417		-1.52564	2.68448		-1.55415	2.71730		-1.52723	2.68902
31.570		0.01033	0.01313		-1.92011	1.94611		-1.94149	1.97136		-1.92678	1.95907
31.575		0.00951	0.01213		-0.54473	0.42726		-0.55757	0.44348		-0.55449	0.44586
31.580		0.00871	0.01119		1.55985	-1.98562		1.55566	-1.97861		1.54923	-1.96442
31.585		0.00795	0.01033		2.15671	-2.72281		2.16005	-2.72393		2.14702	-2.70158
31.590		0.00724	0.00953		3.58017	-3.89263		3.58928	-3.90010		3.57282	-3.87350
31.595		0.00659	0.00879		3.63060	-3.87783		3.64343	-3.88952		3.62652	-3.86238
31.600		0.00601	0.00810		3.33303	-3.43262		3.34744	-3.44629		3.33258	-3.42175
31.605		0.00550	0.00746		2.29374	-2.32226		2.30782	-2.33583		2.29675	-2.31615
31.610		0.00506	0.00686		0.22931	-0.36973		0.24156	-0.38154		0.23521	-0.36806
31.615		0.00467	0.00628		-1.07660	0.97295		-1.06726	0.96407		-1.06876	0.97105
31.620		0.00433	0.00572		-4.04019	3.43356		-4.03425	3.42818		-4.03135	3.42903
31.625		0.00404	0.00517		-4.75799	4.07893		-4.75556	4.07717		-4.74931	4.07301
31.630		0.00377	0.00464		-7.38391	5.90912		-7.38459	5.91056		-7.37618	5.90274
31.635		0.00352	0.00412		-6.87696	5.27387		-6.88016	5.27787		-6.87105	5.26805
31.640		0.00327	0.00361		-6.36867	4.42318		-6.37357	4.42883		-6.36502	4.41850
31.645		0.00303	0.00311		-3.57103	1.79517		-3.57674	1.80152		-3.56987	1.79203
31.650		0.00277	0.00263		-0.67505	-0.86339		-0.68076	-0.85726		-0.67623	-0.86500
31.655		0.00250	0.00215		1.63163	-2.93960		1.62659	-2.93443		1.62852	-2.93993
31.660		0.00222	0.00169		3.10367	-4.17818		3.09974	-4.17453		3.09919	-4.17767
31.665		0.00191	0.00123		3.75000	-4.58290		3.74741	-4.58107		3.74473	-4.58199
31.670		0.00159	0.00078		3.83518	-4.39184		3.83389	-4.39183		3.82969	-4.39098
31.675		0.00125	0.00033		3.43506	-3.71237		3.43493	-3.71402		3.42985	-3.71190
31.680		0.00089	-0.00012		2.69530	-2.70683		2.69602	-2.70981		2.69075	-2.70698
31.685		0.00052	-0.00058		1.77456	-1.54892		1.77578	-1.55277		1.77091	-1.54975
31.690		0.00015	-0.00103		0.82311	-0.40091		0.82449	-0.40516		0.82049	-0.40236
31.695		-0.00023	-0.00150		-0.03397	0.60403		-0.03274	0.59985		-0.03555	0.60213
31.700		-0.00061	-0.00196		-0.30789	1.07032		-0.30704	1.06662		-0.30854	1.06827
31.705		-0.00098	-0.00242		-0.71121	1.59476		-0.71085	1.59183		-0.71105	1.59280
31.710		-0.00135	-0.00288		-1.13144	2.04266		-1.13158	2.04067		-1.13062	2.04103
31.715		-0.00171	-0.00333		-1.30268	2.18534		-1.30323	2.18434		-1.30136	2.18426
31.720		-0.00206	-0.00376		-1.25499	2.06371		-1.25586	2.06369		-1.25337	2.06333
31.725		-0.00240	-0.00417		-1.03642	1.73626		-1.03744	1.73706		-1.03464	1.73664
31.730		-0.00272	-0.00456		-0.70890	1.27593		-0.70989	1.27738		-0.70708	1.27704
31.735		-0.00303	-0.00493		-0.33696	0.75812		-0.33778	0.75999		-0.33519	0.75985
31.740		-0.00331	-0.00526		0.02085	0.25137		0.02032	0.25342		0.02252	0.25355
31.745		-0.00357	-0.00556		0.31826	-0.18946		0.31811	-0.18743		0.31980	-0.18701
31.750		-0.00381	-0.00583		0.52491	-0.52715		0.52515	-0.52533		0.52632	-0.52466
31.755		-0.00403	-0.00606		0.62730	-0.74338		0.62792	-0.74188		0.62859	-0.74101
31.760		-0.00422	-0.00626		1.31593	-1.42975		1.31683	-1.42855		1.31707	-1.42758

		A			B			C			D	
t		$\ddot{u}_1$	$\ddot{u}_2$		$\ddot{u}_1$	$\ddot{u}_2$		$\ddot{u}_1$	$\ddot{u}_2$		$\ddot{u}_1$	$\ddot{u}_2$
(s)		$(m/s)^2$	$(m/s)^2$		$(m/s)^2$	$(m/s)^2$		$(m/s)^2$	$(m/s)^2$		$(m/s)^2$	$(m/s)^2$
31.765		-0.00438	-0.00643		1.45950	-1.56780		1.46066	-1.56694		1.46056	-1.56596
31.770		-0.00452	-0.00657		1.09917	-1.22415		1.10055	-1.22357		1.10022	-1.22266
31.775		-0.00464	-0.00667		0.66016	-0.79550		0.66169	-0.79507		0.66121	-0.79432
31.780		-0.00474	-0.00676		0.21203	-0.35227		0.21364	-0.35182		0.21311	-0.35128
31.785		-0.00481	-0.00681		-0.18874	0.04642		-0.18710	0.04705		-0.18763	0.04734
31.790		-0.00487	-0.00685		-0.50300	0.35926		-0.50136	0.36020		-0.50184	0.36024
31.795		-0.00490	-0.00687		-0.70892	0.56306		-0.70730	0.56442		-0.70771	0.56422
31.800		-0.00492	-0.00687		-0.80144	0.65225		-0.79984	0.65407		-0.80019	0.65367
31.805		-0.00493	-0.00685		-0.78991	0.63638		-0.78834	0.63864		-0.78862	0.63808
31.810		-0.00493	-0.00682		-0.69435	0.53625		-0.69280	0.53886		-0.69304	0.53820
31.815		-0.00491	-0.00677		-0.54115	0.37934		-0.53962	0.38217		-0.53984	0.38145
31.820		-0.00489	-0.00671		-0.35875	0.19527		-0.35725	0.19817		-0.35747	0.19743
31.825		-0.00486	-0.00664		-0.17385	0.01181		-0.17238	0.01460		-0.17263	0.01388
31.830		-0.00483	-0.00656		-0.00851	-0.14817		-0.00709	-0.14565		-0.00738	-0.14634
31.835		-0.00479	-0.00647		0.12168	-0.26858		0.12302	-0.26645		0.12266	-0.26711
31.840		-0.00474	-0.00637		0.20828	-0.34086		0.20950	-0.33923		0.20907	-0.33988
31.845		-0.00469	-0.00626		0.24972	-0.36373		0.25079	-0.36263		0.25027	-0.36330
31.850		-0.00464	-0.00614		0.25022	-0.34200		0.25111	-0.34142		0.25051	-0.34214
31.855		-0.00458	-0.00602		0.21821	-0.28501		0.21889	-0.28490		0.21821	-0.28569
31.860		-0.00451	-0.00589		0.16452	-0.20466		0.16497	-0.20492		0.16421	-0.20581
31.865		-0.00444	-0.00575		0.10062	-0.11356		0.10082	-0.11411		0.10000	-0.11510
31.870		-0.00436	-0.00560		0.03711	-0.02340		0.03707	-0.02412		0.03619	-0.02522
31.875		-0.00427	-0.00545		-0.01741	0.05630		-0.01767	0.05550		-0.01859	0.05430
31.880		-0.00418	-0.00529		-0.05704	0.11893		-0.05749	0.11813		-0.05844	0.11686
31.885		-0.00409	-0.00512		-0.07880	0.16106		-0.07941	0.16033		-0.08038	0.15901
31.890		-0.00399	-0.00495		-0.08249	0.18229		-0.08320	0.18167		-0.08418	0.18031
31.895		-0.00388	-0.00477		-0.07019	0.18475		-0.07094	0.18424		-0.07195	0.18286
31.900		-0.00376	-0.00459		-0.04562	0.17233		-0.04638	0.17194		-0.04739	0.17055
31.905		-0.00364	-0.00441		-0.01339	0.14998		-0.01411	0.14968		-0.01514	0.14828
31.910		-0.00352	-0.00421		0.02169	0.12282		0.02106	0.12258		0.02001	0.12119
31.915		-0.00339	-0.00402		0.05527	0.09553		0.05474	0.09533		0.05369	0.09396
31.920		-0.00326	-0.00382		0.08383	0.07184		0.08343	0.07165		0.08239	0.07029
31.925		-0.00312	-0.00362		0.10502	0.05420		0.10474	0.05400		0.10371	0.05268
31.930		-0.00299	-0.00342		0.11766	0.04376		0.11750	0.04354		0.11650	0.04228
31.935		-0.00284	-0.00321		0.12174	0.04044		0.12168	0.04018		0.12073	0.03899
31.940		-0.00270	-0.00301		0.11818	0.04314		0.11818	0.04285		0.11729	0.04175
31.945		-0.00256	-0.00281		0.10854	0.05012		0.10858	0.04978		0.10777	0.04880
31.950		-0.00241	-0.00260		0.09476	0.05929		0.09479	0.05888		0.09408	0.05805
31.955		-0.00227	-0.00240		0.07883	0.06853		0.07881	0.06805		0.07822	0.06739
31.960		-0.00213	-0.00220		0.06254	0.07601		0.06244	0.07544		0.06198	0.07497
31.965		-0.00198	-0.00201		0.04736	0.08034		0.04715	0.07967		0.04683	0.07939
31.970		-0.00184	-0.00181		0.03428	0.08072		0.03395	0.07993		0.03377	0.07985
31.975		-0.00170	-0.00163		0.02386	0.07693		0.02340	0.07603		0.02337	0.07614
31.980		-0.00157	-0.00144		0.01621	0.06933		0.01561	0.06833		0.01573	0.06862
31.985		-0.00143	-0.00126		0.01112	0.05874		0.01039	0.05764		0.01064	0.05809
31.990		-0.00130	-0.00109		0.00812	0.04623		0.00728	0.04505		0.00765	0.04564
31.995		-0.00117	-0.00091		0.00662	0.03302		0.00569	0.03178		0.00617	0.03248
32.000		-0.00105	-0.00075		0.00603	0.02025		0.00502	0.01896		0.00559	0.01975
32.005		-0.00092	-0.00059		0.00575	0.00884		0.00470	0.00755		0.00534	0.00838
32.010		-0.00080	-0.00044		0.00533	-0.00055		0.00426	-0.00184		0.00495	-0.00097
32.015		-0.00069	-0.00029		0.00446	-0.00763		0.00339	-0.00890		0.00411	-0.00801
32.020		-0.00058	-0.00014		0.00298	-0.01240		0.00194	-0.01362		0.00267	-0.01274

	A		B		C		D	
t	$\ddot{u}_1$	$\ddot{u}_2$	$\ddot{u}_1$	$\ddot{u}_2$	$\ddot{u}_1$	$\ddot{u}_2$	$\ddot{u}_1$	$\ddot{u}_2$
(s)	$(m/s)^2$	$(m/s)^2$	$(m/s)^2$	$(m/s)^2$	$(m/s)^2$	$(m/s)^2$	$(m/s)^2$	$(m/s)^2$
32.025	-0.00047	-0.00001	0.00093	-0.01508	-0.00007	-0.01624	0.00065	-0.01538
32.030	-0.00037	0.00012	-0.00154	-0.01603	-0.00248	-0.01712	-0.00178	-0.01629
32.035	-0.00027	0.00025	-0.00415	-0.01568	-0.00502	-0.01670	-0.00436	-0.01590
32.040	-0.00017	0.00037	-0.00658	-0.01440	-0.00738	-0.01534	-0.00677	-0.01459
32.045	-0.00008	0.00048	-0.00851	-0.01250	-0.00922	-0.01337	-0.00866	-0.01265
32.050	0.00001	0.00059	-0.00962	-0.01015	-0.01026	-0.01095	-0.00976	-0.01027
32.055	0.00010	0.00069	-0.00971	-0.00743	-0.01028	-0.00816	-0.00982	-0.00752
32.060	0.00018	0.00079	-0.00866	-0.00435	-0.00915	-0.00502	-0.00875	-0.00442
32.065	0.00026	0.00088	-0.00647	-0.00092	-0.00691	-0.00153	-0.00655	-0.00097
32.070	0.00033	0.00097	-0.00331	0.00281	-0.00370	0.00225	-0.00338	0.00279
32.075	0.00040	0.00105	0.00058	0.00671	0.00024	0.00621	0.00053	0.00671
32.080	0.00047	0.00112	0.00490	0.01062	0.00460	0.01016	0.00486	0.01064
32.085	0.00053	0.00119	0.00931	0.01430	0.00903	0.01388	0.00929	0.01434
32.090	0.00059	0.00125	0.01349	0.01753	0.01324	0.01716	0.01349	0.01760
32.095	0.00065	0.00131	0.01719	0.02013	0.01695	0.01979	0.01720	0.02023
32.100	0.00070	0.00136	0.02017	0.02193	0.01995	0.02162	0.02020	0.02205
32.105	0.00075	0.00141	0.02229	0.02284	0.02208	0.02257	0.02233	0.02299
32.110	0.00080	0.00145	0.02346	0.02283	0.02326	0.02258	0.02353	0.02301
32.115	0.00084	0.00149	0.02366	0.02192	0.02347	0.02170	0.02376	0.02213
32.120	0.00088	0.00152	0.02294	0.02020	0.02275	0.02001	0.02305	0.02044
32.125	0.00091	0.00155	0.02134	0.01779	0.02117	0.01762	0.02148	0.01806
32.130	0.00094	0.00158	0.01901	0.01482	0.01884	0.01468	0.01917	0.01512
32.135	0.00097	0.00159	0.01606	0.01145	0.01590	0.01133	0.01624	0.01178
32.140	0.00099	0.00161	0.01266	0.00783	0.01252	0.00773	0.01287	0.00818
32.145	0.00101	0.00162	0.00897	0.00411	0.00884	0.00403	0.00920	0.00449
32.150	0.00103	0.00163	0.00516	0.00041	0.00505	0.00036	0.00541	0.00081
32.155	0.00104	0.00163	0.00136	-0.00315	0.00128	-0.00318	0.00163	-0.00274
32.160	0.00106	0.00163	-0.00228	-0.00651	-0.00235	-0.00652	-0.00199	-0.00608
32.165	0.00107	0.00162	-0.00566	-0.00961	-0.00571	-0.00959	-0.00536	-0.00917
32.170	0.00107	0.00161	-0.00871	-0.01242	-0.00873	-0.01237	-0.00840	-0.01197
32.175	0.00108	0.00160	-0.01137	-0.01492	-0.01137	-0.01484	-0.01105	-0.01446
32.180	0.00108	0.00159	-0.01360	-0.01712	-0.01358	-0.01701	-0.01328	-0.01666
32.185	0.00108	0.00157	-0.01543	-0.01905	-0.01538	-0.01891	-0.01510	-0.01858
32.190	0.00108	0.00155	-0.01686	-0.02072	-0.01679	-0.02055	-0.01653	-0.02026
32.195	0.00107	0.00153	-0.01793	-0.02216	-0.01784	-0.02196	-0.01760	-0.02170
32.200	0.00107	0.00151	-0.01868	-0.02338	-0.01856	-0.02316	-0.01835	-0.02293
32.205	0.00106	0.00149	-0.01915	-0.02439	-0.01901	-0.02414	-0.01882	-0.02393
32.210	0.00105	0.00146	-0.01938	-0.02516	-0.01922	-0.02489	-0.01906	-0.02472
32.215	0.00104	0.00143	-0.01940	-0.02569	-0.01922	-0.02540	-0.01908	-0.02526
32.220	0.00103	0.00140	-0.01925	-0.02597	-0.01905	-0.02565	-0.01894	-0.02554
32.225	0.00101	0.00137	-0.01896	-0.02598	-0.01875	-0.02565	-0.01865	-0.02556
32.230	0.00100	0.00134	-0.01855	-0.02573	-0.01832	-0.02539	-0.01825	-0.02532
32.235	0.00098	0.00130	-0.01805	-0.02524	-0.01781	-0.02488	-0.01776	-0.02484
32.240	0.00097	0.00127	-0.01748	-0.02454	-0.01723	-0.02417	-0.01719	-0.02415
32.245	0.00095	0.00124	-0.01685	-0.02366	-0.01660	-0.02328	-0.01657	-0.02328
32.250	0.00093	0.00120	-0.01619	-0.02266	-0.01593	-0.02228	-0.01592	-0.02229
32.255	0.00091	0.00117	-0.01551	-0.02158	-0.01524	-0.02120	-0.01524	-0.02123
32.260	0.00090	0.00113	-0.01482	-0.02049	-0.01455	-0.02011	-0.01456	-0.02015
32.265	0.00088	0.00110	-0.01414	-0.01943	-0.01386	-0.01904	-0.01388	-0.01909
32.270	0.00086	0.00106	-0.01348	-0.01843	-0.01321	-0.01804	-0.01323	-0.01811
32.275	0.00084	0.00102	-0.01286	-0.01753	-0.01259	-0.01714	-0.01262	-0.01722
32.280	0.00082	0.00099	-0.01229	-0.01674	-0.01202	-0.01636	-0.01205	-0.01644

		A			B			C			D	
t		$\ddot{u}_1$	$\ddot{u}_2$		$\ddot{u}_1$	$\ddot{u}_2$		$\ddot{u}_1$	$\ddot{u}_2$		$\ddot{u}_1$	$\ddot{u}_2$
(s)		$(m/s)^2$	$(m/s)^2$		$(m/s)^2$	$(m/s)^2$		$(m/s)^2$	$(m/s)^2$		$(m/s)^2$	$(m/s)^2$
32.285		0.00080	0.00095		-0.01178	-0.01607		-0.01150	-0.01568		-0.01155	-0.01577
32.290		0.00078	0.00092		-0.01133	-0.01550		-0.01106	-0.01511		-0.01110	-0.01521
32.295		0.00076	0.00088		-0.01095	-0.01502		-0.01068	-0.01464		-0.01073	-0.01475
32.300		0.00074	0.00085		-0.01064	-0.01461		-0.01037	-0.01424		-0.01043	-0.01435
32.305		0.00072	0.00082		-0.01039	-0.01425		-0.01012	-0.01388		-0.01018	-0.01400
32.310		0.00070	0.00079		-0.01019	-0.01391		-0.00992	-0.01354		-0.00999	-0.01367
32.315		0.00068	0.00075		-0.01003	-0.01357		-0.00977	-0.01321		-0.00984	-0.01334
32.320		0.00066	0.00072		-0.00990	-0.01321		-0.00964	-0.01286		-0.00971	-0.01300
32.325		0.00064	0.00069		-0.00978	-0.01282		-0.00952	-0.01247		-0.00960	-0.01262
32.330		0.00062	0.00066		-0.00965	-0.01239		-0.00939	-0.01204		-0.00948	-0.01219
32.335		0.00060	0.00064		-0.00950	-0.01191		-0.00924	-0.01157		-0.00934	-0.01173
32.340		0.00058	0.00061		-0.00931	-0.01138		-0.00906	-0.01106		-0.00916	-0.01122
32.345		0.00057	0.00058		-0.00908	-0.01082		-0.00884	-0.01050		-0.00894	-0.01067
32.350		0.00055	0.00056		-0.00881	-0.01022		-0.00856	-0.00990		-0.00867	-0.01008
32.355		0.00054	0.00053		-0.00847	-0.00959		-0.00823	-0.00928		-0.00835	-0.00946
32.360		0.00052	0.00051		-0.00808	-0.00893		-0.00785	-0.00864		-0.00797	-0.00882
32.365		0.00050	0.00049		-0.00764	-0.00826		-0.00742	-0.00797		-0.00754	-0.00816
32.370		0.00049	0.00047		-0.00716	-0.00757		-0.00694	-0.00730		-0.00706	-0.00749
32.375		0.00048	0.00045		-0.00664	-0.00688		-0.00642	-0.00661		-0.00655	-0.00680
32.380		0.00046	0.00043		-0.00609	-0.00618		-0.00588	-0.00592		-0.00601	-0.00612
32.385		0.00045	0.00041		-0.00552	-0.00548		-0.00531	-0.00523		-0.00545	-0.00543
32.390		0.00044	0.00039		-0.00494	-0.00478		-0.00474	-0.00454		-0.00488	-0.00474
32.395		0.00043	0.00038		-0.00436	-0.00408		-0.00417	-0.00386		-0.00430	-0.00405
32.400		0.00042	0.00036		-0.00378	-0.00339		-0.00360	-0.00318		-0.00374	-0.00337
32.405		0.00041	0.00035		-0.00322	-0.00271		-0.00305	-0.00251		-0.00319	-0.00269
32.410		0.00040	0.00034		-0.00268	-0.00204		-0.00252	-0.00185		-0.00265	-0.00203
32.415		0.00039	0.00032		-0.00217	-0.00138		-0.00201	-0.00121		-0.00214	-0.00139
32.420		0.00038	0.00031		-0.00167	-0.00075		-0.00152	-0.00059		-0.00166	-0.00077
32.425		0.00037	0.00030		-0.00121	-0.00015		-0.00107	0.00001		-0.00120	-0.00017
32.430		0.00037	0.00030		-0.00077	0.00043		-0.00064	0.00058		-0.00077	0.00040
32.435		0.00036	0.00029		-0.00036	0.00098		-0.00023	0.00111		-0.00036	0.00094
32.440		0.00035	0.00028		0.00003	0.00149		0.00014	0.00161		0.00002	0.00145
32.445		0.00035	0.00027		0.00039	0.00197		0.00049	0.00208		0.00037	0.00192
32.450		0.00034	0.00027		0.00072	0.00241		0.00082	0.00251		0.00071	0.00235
32.455		0.00034	0.00026		0.00103	0.00281		0.00113	0.00290		0.00101	0.00275
32.460		0.00033	0.00026		0.00132	0.00318		0.00141	0.00326		0.00130	0.00312
32.465		0.00033	0.00025		0.00159	0.00352		0.00167	0.00359		0.00156	0.00345
32.470		0.00032	0.00025		0.00184	0.00382		0.00191	0.00388		0.00181	0.00375
32.475		0.00032	0.00025		0.00207	0.00410		0.00214	0.00415		0.00204	0.00403
32.480		0.00032	0.00025		0.00228	0.00435		0.00234	0.00440		0.00225	0.00428
32.485		0.00031	0.00024		0.00248	0.00459		0.00253	0.00462		0.00244	0.00450
32.490		0.00031	0.00024		0.00267	0.00480		0.00271	0.00482		0.00262	0.00471
32.495		0.00031	0.00024		0.00284	0.00499		0.00287	0.00501		0.00279	0.00490
32.500		0.00031	0.00024		0.00299	0.00517		0.00302	0.00517		0.00294	0.00508
32.505		0.00030	0.00024		0.00314	0.00533		0.00317	0.00533		0.00309	0.00523
32.510		0.00030	0.00024		0.00328	0.00547		0.00330	0.00547		0.00322	0.00538
32.515		0.00030	0.00024		0.00340	0.00560		0.00342	0.00559		0.00334	0.00551
32.520		0.00030	0.00024		0.00352	0.00572		0.00353	0.00570		0.00346	0.00562
32.525		0.00030	0.00024		0.00363	0.00582		0.00363	0.00580		0.00357	0.00572
32.530		0.00030	0.00024		0.00373	0.00591		0.00373	0.00588		0.00367	0.00581
32.535		0.00029	0.00024		0.00382	0.00598		0.00381	0.00594		0.00376	0.00588
32.540		0.00029	0.00024		0.00390	0.00604		0.00389	0.00599		0.00384	0.00594

		A			B			C			D	
t		$\ddot{u}_1$	$\ddot{u}_2$		$\ddot{u}_1$	$\ddot{u}_2$		$\ddot{u}_1$	$\ddot{u}_2$		$\ddot{u}_1$	$\ddot{u}_2$
(s)		$(m/s)^2$	$(m/s)^2$		$(m/s)^2$	$(m/s)^2$		$(m/s)^2$	$(m/s)^2$		$(m/s)^2$	$(m/s)^2$
32.545		0.00029	0.00024		0.00397	0.00608		0.00396	0.00603		0.00391	0.00598
32.550		0.00029	0.00024		0.00403	0.00610		0.00402	0.00605		0.00397	0.00600
32.555		0.00029	0.00024		0.00409	0.00611		0.00406	0.00605		0.00402	0.00601
32.560		0.00029	0.00024		0.00413	0.00610		0.00410	0.00604		0.00406	0.00601
32.565		0.00028	0.00024		0.00416	0.00608		0.00413	0.00602		0.00409	0.00599
32.570		0.00028	0.00024		0.00417	0.00605		0.00414	0.00598		0.00411	0.00595
32.575		0.00028	0.00024		0.00418	0.00600		0.00414	0.00593		0.00411	0.00590
32.580		0.00028	0.00024		0.00417	0.00593		0.00413	0.00586		0.00411	0.00584
32.585		0.00027	0.00024		0.00415	0.00586		0.00411	0.00578		0.00409	0.00576
32.590		0.00027	0.00024		0.00412	0.00577		0.00408	0.00569		0.00406	0.00568
32.595		0.00027	0.00024		0.00408	0.00566		0.00404	0.00558		0.00402	0.00558
32.600		0.00027	0.00023		0.00403	0.00555		0.00399	0.00547		0.00397	0.00547
32.605		0.00026	0.00023		0.00397	0.00543		0.00392	0.00535		0.00391	0.00535
32.610		0.00026	0.00023		0.00390	0.00530		0.00385	0.00521		0.00385	0.00522
32.615		0.00026	0.00023		0.00383	0.00516		0.00378	0.00507		0.00377	0.00508
32.620		0.00025	0.00022		0.00375	0.00501		0.00369	0.00492		0.00369	0.00493
32.625		0.00025	0.00022		0.00366	0.00485		0.00360	0.00477		0.00360	0.00478
32.630		0.00024	0.00022		0.00356	0.00469		0.00351	0.00460		0.00351	0.00462
32.635		0.00024	0.00021		0.00346	0.00452		0.00341	0.00444		0.00341	0.00446
32.640		0.00023	0.00021		0.00336	0.00435		0.00330	0.00427		0.00331	0.00429
32.645		0.00023	0.00020		0.00325	0.00418		0.00320	0.00409		0.00320	0.00412
32.650		0.00022	0.00020		0.00314	0.00400		0.00309	0.00392		0.00309	0.00394
32.655		0.00022	0.00019		0.00303	0.00382		0.00297	0.00374		0.00298	0.00377
32.660		0.00021	0.00019		0.00292	0.00364		0.00286	0.00356		0.00287	0.00359
32.665		0.00020	0.00018		0.00280	0.00346		0.00275	0.00338		0.00276	0.00341
32.670		0.00020	0.00017		0.00269	0.00329		0.00263	0.00320		0.00265	0.00323
32.675		0.00019	0.00017		0.00257	0.00311		0.00252	0.00303		0.00253	0.00306
32.680		0.00018	0.00016		0.00246	0.00293		0.00240	0.00285		0.00242	0.00288
32.685		0.00018	0.00015		0.00234	0.00275		0.00229	0.00268		0.00230	0.00271
32.690		0.00017	0.00014		0.00223	0.00258		0.00217	0.00250		0.00219	0.00254
32.695		0.00016	0.00013		0.00211	0.00241		0.00206	0.00233		0.00208	0.00237
32.700		0.00015	0.00013		0.00200	0.00224		0.00195	0.00217		0.00197	0.00220
32.705		0.00014	0.00012		0.00189	0.00207		0.00184	0.00200		0.00186	0.00204
32.710		0.00014	0.00011		0.00178	0.00191		0.00173	0.00184		0.00175	0.00188
32.715		0.00013	0.00010		0.00167	0.00175		0.00162	0.00168		0.00164	0.00172
32.720		0.00012	0.00009		0.00156	0.00160		0.00151	0.00153		0.00153	0.00157
32.725		0.00011	0.00008		0.00145	0.00144		0.00141	0.00138		0.00143	0.00142
32.730		0.00010	0.00007		0.00135	0.00130		0.00130	0.00124		0.00133	0.00127
32.735		0.00009	0.00006		0.00125	0.00115		0.00120	0.00109		0.00123	0.00113
32.740		0.00008	0.00005		0.00115	0.00101		0.00111	0.00096		0.00113	0.00099
32.745		0.00007	0.00004		0.00105	0.00088		0.00101	0.00083		0.00103	0.00086
32.750		0.00006	0.00003		0.00096	0.00075		0.00092	0.00070		0.00094	0.00073
32.755		0.00005	0.00002		0.00087	0.00063		0.00083	0.00058		0.00085	0.00061
32.760		0.00004	0.00000		0.00078	0.00051		0.00074	0.00046		0.00076	0.00049
32.765		0.00003	-0.00001		0.00070	0.00039		0.00066	0.00035		0.00068	0.00038
32.770		0.00002	-0.00002		0.00061	0.00028		0.00058	0.00024		0.00060	0.00027
32.775		0.00001	-0.00003		0.00053	0.00018		0.00050	0.00014		0.00052	0.00017
32.780		0.00000	-0.00004		0.00046	0.00008		0.00042	0.00004		0.00044	0.00007
32.785		-0.00001	-0.00005		0.00039	-0.00001		0.00035	-0.00005		0.00037	-0.00002
32.790		-0.00002	-0.00006		0.00032	-0.00010		0.00028	-0.00013		0.00030	-0.00011
32.795		-0.00003	-0.00007		0.00025	-0.00018		0.00022	-0.00021		0.00024	-0.00019
32.800		-0.00004	-0.00008		0.00019	-0.00025		0.00016	-0.00029		0.00018	-0.00026

		A			B			C			D	
t		$\ddot{u}_1$	$\ddot{u}_2$		$\ddot{u}_1$	$\ddot{u}_2$		$\ddot{u}_1$	$\ddot{u}_2$		$\ddot{u}_1$	$\ddot{u}_2$
(s)		$(m/s)^2$	$(m/s)^2$		$(m/s)^2$	$(m/s)^2$		$(m/s)^2$	$(m/s)^2$		$(m/s)^2$	$(m/s)^2$
32.805		-0.00005	-0.00010		0.00013	-0.00032		0.00010	-0.00036		0.00012	-0.00033
32.810		-0.00006	-0.00011		0.00008	-0.00039		0.00005	-0.00042		0.00007	-0.00040
32.815		-0.00007	-0.00012		0.00003	-0.00045		0.00000	-0.00048		0.00002	-0.00045
32.820		-0.00008	-0.00013		-0.00002	-0.00050		-0.00004	-0.00053		-0.00003	-0.00051
32.825		-0.00009	-0.00014		-0.00006	-0.00055		-0.00009	-0.00058		-0.00007	-0.00056
32.830		-0.00010	-0.00015		-0.00010	-0.00059		-0.00013	-0.00062		-0.00011	-0.00060
32.835		-0.00011	-0.00016		-0.00014	-0.00063		-0.00016	-0.00066		-0.00015	-0.00064
32.840		-0.00012	-0.00017		-0.00017	-0.00067		-0.00019	-0.00069		-0.00018	-0.00067
32.845		-0.00013	-0.00018		-0.00020	-0.00069		-0.00022	-0.00071		-0.00021	-0.00070
32.850		-0.00013	-0.00019		-0.00022	-0.00072		-0.00025	-0.00074		-0.00023	-0.00072
32.855		-0.00014	-0.00020		-0.00025	-0.00074		-0.00027	-0.00076		-0.00026	-0.00074
32.860		-0.00015	-0.00021		-0.00027	-0.00075		-0.00029	-0.00077		-0.00028	-0.00076
32.865		-0.00016	-0.00022		-0.00028	-0.00076		-0.00030	-0.00078		-0.00029	-0.00077
32.870		-0.00017	-0.00023		-0.00030	-0.00077		-0.00032	-0.00079		-0.00031	-0.00078
32.875		-0.00018	-0.00024		-0.00031	-0.00077		-0.00033	-0.00079		-0.00032	-0.00078
32.880		-0.00019	-0.00025		-0.00032	-0.00077		-0.00034	-0.00079		-0.00033	-0.00078
32.885		-0.00019	-0.00025		-0.00032	-0.00077		-0.00034	-0.00079		-0.00033	-0.00078
32.890		-0.00020	-0.00026		-0.00033	-0.00076		-0.00035	-0.00078		-0.00034	-0.00077
32.895		-0.00021	-0.00027		-0.00033	-0.00076		-0.00035	-0.00077		-0.00034	-0.00076
32.900		-0.00021	-0.00028		-0.00033	-0.00074		-0.00035	-0.00076		-0.00034	-0.00075
32.905		-0.00022	-0.00028		-0.00033	-0.00073		-0.00034	-0.00074		-0.00034	-0.00074
32.910		-0.00023	-0.00029		-0.00032	-0.00071		-0.00034	-0.00072		-0.00033	-0.00072
32.915		-0.00023	-0.00030		-0.00032	-0.00069		-0.00033	-0.00070		-0.00033	-0.00070
32.920		-0.00024	-0.00030		-0.00031	-0.00067		-0.00033	-0.00068		-0.00032	-0.00068
32.925		-0.00025	-0.00031		-0.00030	-0.00065		-0.00032	-0.00066		-0.00031	-0.00066
32.930		-0.00025	-0.00031		-0.00029	-0.00062		-0.00031	-0.00064		-0.00030	-0.00063
32.935		-0.00026	-0.00032		-0.00028	-0.00060		-0.00030	-0.00061		-0.00029	-0.00061
32.940		-0.00026	-0.00032		-0.00027	-0.00057		-0.00028	-0.00058		-0.00028	-0.00058
32.945		-0.00027	-0.00033		-0.00025	-0.00054		-0.00027	-0.00055		-0.00027	-0.00055
32.950		-0.00027	-0.00033		-0.00024	-0.00051		-0.00025	-0.00052		-0.00025	-0.00052
32.955		-0.00027	-0.00033		-0.00022	-0.00048		-0.00024	-0.00049		-0.00024	-0.00049
32.960		-0.00028	-0.00034		-0.00021	-0.00045		-0.00022	-0.00046		-0.00022	-0.00046
32.965		-0.00028	-0.00034		-0.00019	-0.00042		-0.00021	-0.00043		-0.00021	-0.00043
32.970		-0.00028	-0.00034		-0.00018	-0.00039		-0.00019	-0.00040		-0.00019	-0.00040
32.975		-0.00029	-0.00034		-0.00016	-0.00036		-0.00017	-0.00037		-0.00017	-0.00037